Summary Correspondences

No.	Hal	Tanggal
1	Submit Jurnal	11 November 2025
2	Reviewer meminta revisi	23 Januari 2026
3	Response terhadap komentar reviewer	9 Februari 2026
4	Submit Revisi	17 Februari 2026
5	Accepted	11 Maret 2026
6	Permintaan untuk Proof Edit	24 Maret 2026
7	Hasil Proof Edit	24 Maret 2026
8	Tersedia dalam Online	13 April 2026

Submission Confirmation for Molecular-Glass Interface Engineering Enables Highly Efficient and Stable Inverted Perovskite Solar Cells (ente.202502597)

External Inbox × Updates ×

EnergyTechnology <em@editorialmanager.com>
to me

Nov 17, 2025, 2:05 PM

You are being blind carbon copied ("bcc:'d") on an e-mail "To" "Md. Shahiduzzaman" shahiduzzaman09@gmail.com

Dear Dr. Shahiduzzaman,

Your submission entitled "Molecular-Glass Interface Engineering Enables Highly Efficient and Stable Inverted Perovskite Solar Cells" has been received by journal Energy Technology. The manuscript number for your submission is ente.202502597.

To view your submission, please login to https://www.editorialmanager.com/ente/ by entering your username (********) and password and selecting the "Author Login" option.

If the manuscript is accepted for publication, this author's affiliation will be used to determine eligibility for some open access funding (click here for details).

This journal offers a number of license options; information about this is available here. The submitting author has confirmed that all co-authors have the necessary rights to grant in the submission, including in light of each co-author's funder's policies. If any author's funder has a policy that restricts which kinds of license they can sign, for example if the funder is a member of Coalition S, please make sure the submitting author is aware.

This message has been sent to all named co-authors listed in the submission process to serve as notification of submission.

Thank you for submitting your work to the journal.

Kind regards,

Editorial Office

Energy Technology
E-mail: energy-technology@wiley.com

Sohel Sensei
last seen today at 7:20 ...

manuscript draft.

6:33 PM

1/23/2026

COMMENTS TO AUTHOR:

Reviewer #1: The manuscript, entitled "Molecular-Glass Interface Engineering Enables Highly Efficient and Stable Inverted Perovskite Solar Cells," presents interface engineering for a MAPbI3-based inverted solar cell design aimed at improving its performance and stability. The work demonstrates that incorporating FFI 1, FFI 2, and DPP 3 between the perovskite absorber and PCBM improves its photovoltaic performance, while also enhancing its hydrophobicity and temperature stability to a slight extent. The work is well presented and supported by experimental evidence. Only in a few places do the figure axis values need to be properly written.

Reviewer #2: This manuscript reports the use of glass-forming molecular electron-acceptor interlayers (FFI-1, FFI-2, and DPP-3) to enhance the efficiency and thermal stability of inverted (p-i-n) $MAPbI_3$ perovskite solar cells. The topic is timely and potentially relevant to the perovskite photovoltaics community. However, in its current form, the manuscript suffers from deficiencies in experimental details, data support, figure quality, and scholarly rigor. Substantial revision and additional experimental evidence would be required before the work could be considered for publication.

1. Essential characterization details are missing or incomplete, particularly for XRD, UV-Vis, and J-V/MPPT measurements. Instrument models, measurement parameters, calibration procedures, and testing protocols should be clearly reported to ensure

Type a message

3

Author's Responses to Reviewers

We deeply appreciate receiving your letter dated January 23rd, 2026, regarding our manuscript (ente.202502597; Title: *Molecular-Glass Interface Engineering Enables Highly Efficient and Stable Inverted Perovskite Solar Cells*) and the accompanying comments. Your feedback has been very valuable and helpful for improving the quality of the manuscript and aligning it with the requirement of *Energy Technology*. We have address your specific comments as much as possible in our response. Please kindly find the below shown response to the reviewer's suggestion.

Response to the comments

Reviewer #1

Comments:

The manuscript, entitled "*Molecular-Glass Interface Engineering Enables Highly Efficient and Stable Inverted Perovskite Solar Cells*," presents interface engineering for a $MAPbI_3$-based inverted solar cell design aimed at improving its performance and stability. The work demonstrates that incorporating FFI 1, FFI 2, and DPP 3 between the perovskite absorber and PCBM improves its photovoltaic performance, while also enhancing its hydrophobicity and temperature stability to a slight extent. The work is well presented and supported by experimental evidence. Only in a few places do the figure axis values need to be properly written.

Response:

We sincerely thank the reviewer for the positive and encouraging assessment of our manuscript. We greatly appreciate the recognition of the significance of our interface engineering strategy and the experimental evidence supporting the improved efficiency and stability of the devices. In response to the reviewer's comment, we have carefully revised the manuscript to correct and standardize all figure axis labels, units, and numerical values to ensure clarity and readability. We believe these revisions further enhance the quality and presentation of the manuscript.

Reviewer #2

Comments:

This manuscript reports the use of glass-forming molecular electron-acceptor interlayers (FFI-1, FFI-2, and DPP-3) to enhance the efficiency and thermal stability of inverted (p-i-n) $MAPbI_3$ perovskite solar cells. The topic is timely and potentially relevant to the perovskite photovoltaics community. However, in its current form, the manuscript suffers from deficiencies in experimental details, data support, figure quality, and scholarly

rigor. Substantial revision and additional experimental evidence would be required before the work could be considered for publication.

Response:

We thank the reviewer for the detailed and constructive comments. In response to the reviewer's comment, we have considerably revised the manuscript by expanding the experimental details, adding supporting data, improving figure quality, and strengthening the scientific discussion. We believe these revisions address the concerns raised and significantly enhance the rigor and clarity of the work.

Question 1:

Essential characterization details are missing or incomplete, particularly for XRD, UV-Vis, and J-V/MPPT measurements. Instrument models, measurement parameters, calibration procedures, and testing protocols should be clearly reported to ensure reproducibility and allow proper assessment of the results.

Answer 1:

We thank the reviewer for this insightful comment and fully agree that detailed characterization information is essential for reproducibility and clarity. We have revised the manuscript and added a comprehensive **Experimental section** to the Supporting Information, providing complete details of the characterization methods used. The relevant information is summarized below:

- **XRD Spectra:**

  Crystallinity and structural analyses were performed using a Rigaku SmartLab X-ray diffractometer (Japan) equipped with a Cu Kα monochromator (λ = 1.5405 Å), a thin-film collimator, and a fixed incidence angle of 2°. Measurements were carried out at an accelerating voltage of 40 kV and a current of 100 mA, with 2θ scanned from 10° to 60°.

- **UV–Vis Spectra:**

  UV–Vis absorption spectra were recorded using an Agilent Cary 8454 spectrophotometer over a wavelength range of 190-1100 nm. Measurements were conducted on films deposited on FTO/NiOx substrates.

- **J–V and MPPT:**

  Current density-voltage (J-V) and maximum power point tracking (MPPT) measurements were performed using an OTENTO-SUN V solar simulator under AM 1.5G illumination with an intensity of 100 mW cm^{-2} (1 Sun). A xenon lamp

was used as the light source with vertical illumination. J-V scans were conducted with a scan speed of 50 ms, and MPPT measurements were recorded for 300 s.

We believe that the inclusion of these detailed experimental conditions addresses the reviewer's concern and significantly improves the clarity, reproducibility, and scientific rigor of the manuscript.

Question 2:

Several key claims in the Introduction are either unsupported or insufficiently referenced. For example, the statement: "However, despite these advantages, EDA suffers from several drawbacks: its volatile and corrosive nature, combined with limited long-term stability, significantly restricts its practical application." is presented without citation. Such claims require direct literature support, particularly when positioning the present work as an "advantageous alternative." The manuscript frequently cites large blocks of references without clearly attributing specific claims. For instance: "These molecular glass derivatives are especially appealing due to their strong π-bonding, extended delocalization, and inherent hydrophobic properties… (Refs. 25-34)" This citation practice is overly generic and does not clarify which references support which specific properties. References should be cited more selectively and precisely.

Answer 2:

We thank the reviewer for the constructive comments and fully agree that precise statements supported by appropriate references are essential for scholarly rigor. We have thoroughly revised the Introduction to improve specificity, accuracy, and citation quality. Generic or insufficiently supported statements have been corrected and relevant literature has been carefully added where appropriate. Key revisions include the following:

- **Ethylenediamine (EDA):**

  Statements regarding the role of ethylenediamine were revised to more accurately reflect both its benefits and limitations with additional references provided to support these claims. The revised text now reads:

  "Although ethylenediamine (EDA) has been reported to reduce interfacial trap states and facilitate charge extraction in perovskite-based devices, its practical applicability remains constrained by intrinsic material limitations including high volatility, strong chemical reactivity, and well-documented corrosive and sensitizing properties, which raise concerns regarding handling safety and long-term interfacial stability [25–28]."

- **TiO_2 in p–i–n device architectures:**

The discussion of TiO_2 was corrected and expanded with appropriate citations to clarify its limited applicability in inverted architectures. The revised statement reads:
"Despite its widespread use in conventional n–i–p PSCs, TiO_2 is rarely employed in inverted p–i–n architectures due to its requirement for high-temperature processing, unfavorable interfacial energetics, and photocatalytic activity, all of which are incompatible with temperature-sensitive perovskite and hole-transport layers [7–11]."

- **π–π interactions in ligand-engineered interfaces:**

  Statements related to π–π interactions between aromatic ligands and the perovskite surface were refined and supported with targeted references. The revised text reads:
  "In ligand-engineered PSCs, π–π interactions between aromatic moieties of multivalent ligands and the perovskite surface can enhance interfacial ordering and stability by promoting more uniform low-dimensional passivation layers, which contribute to improved defect passivation and charge transport properties [29]."

We believe that these revisions significantly improve the accuracy, specificity, and citation rigor of the Introduction, thereby addressing the reviewer's concern and strengthening the overall scholarly quality of the manuscript.

Questions 3:

The photographs in Figure 4 show minimal visual contrast between pristine and modified perovskite films over aging time. In addition, the pristine perovskite film at 0 h appears unusually pale. Typically, $MAPbI_3$ films are much darker. The authors should clarify imaging conditions and provide clearer or more representative images.

Answer 3:

We thank the reviewer for raising this point regarding the visual appearance of the pristine $MAPbI_3$ film in **Figure 4**. The dark pale or greyish appearance of solution-processed $MAPbI_3$ films, which are fully converted to the perovskite phase after annealing at 100 °C, does not indicate poor film quality; instead, high crystallinity and uniform morphology are confirmed by XRD and SEM analyses (Main Manuscript; **Figures 5 and 8**). The pale appearance of the $MAPbI_3$ films can be partially attributed to the underlying NiO_x layer, perovskite film thickness, substrate reflectivity, and illumination conditions during photography and therefore does not directly correlate with perovskite phase purity or crystallinity.

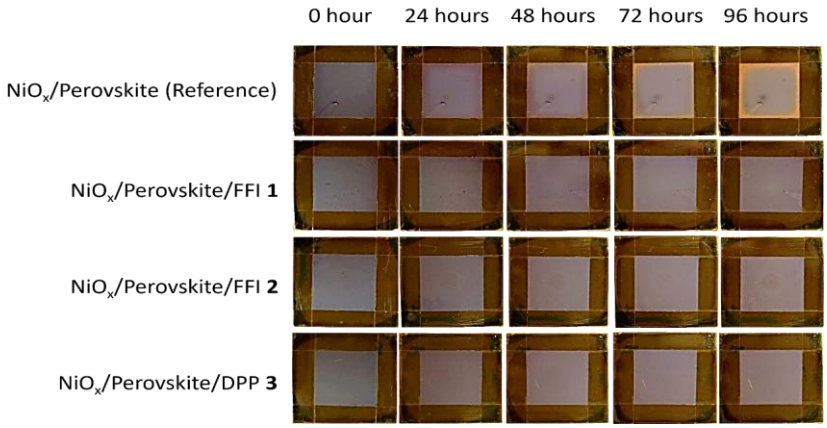

Figure 4. The appearance of perovskite with and without FFI 1, 2, and DPP 3 compounds on thermal stability test.

Question 4:

The XRD patterns appear dominated by the δ-phase for all samples, while the α-phase peaks are relatively weak. This observation is difficult to reconcile with the reported device performance and claims of preserved photoactive phase. Further clarification and careful discussion of phase identification and intensity normalization are needed.

Answer 4:

We thank the reviewer for the comment regarding the interpretation of the XRD spectra. We have clarified that all XRD patterns are plotted using identical intensity normalization enabling direct and consistent comparison of phase evolution over aging time. Although reflections associated with the δ-phase are detectable, the characteristic α-phase $MAPbI_3$ peaks at $2\theta \approx 14.0°$ and $20.1°$ remain clearly present, particularly in the molecular-glass-modified samples. These α-phase reflections confirm the retention of the photoactive perovskite phase that is responsible for the observed device performance. Importantly, compared to the pristine reference, the growth of the PbI_2-related diffraction peak is significantly suppressed in the molecular glass-modified films, indicating improved phase stability and reduced perovskite decomposition. This structural stabilization is consistent with the enhanced efficiency and thermal stability reported. The XRD discussion has been revised accordingly to explicitly clarify phase identification, normalization methodology, and the correlation between structural evolution and device performance.

We believe these revisions address the reviewer's concern and improve the clarity and accuracy of the structural analysis.

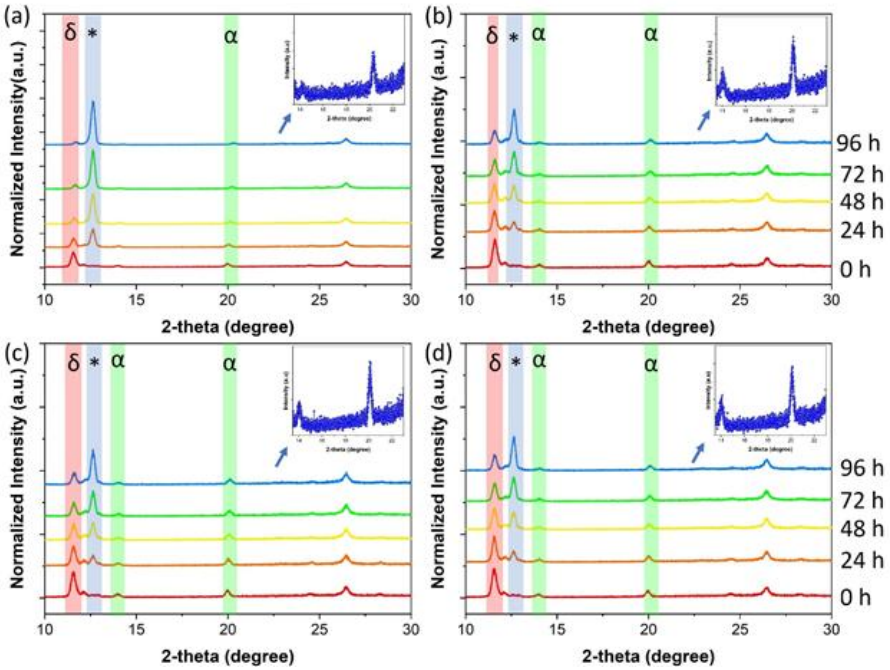

Figure 5. The XRD pattern of pristine perovskite on thermal stability as a (a) reference compared with perovskite added with (b) FFI **1**, (c) FFI **2**, and (d) DPP **3**.

Question 5:

The claim that FFI-modified devices retain over 90% of their initial PCE after 96 hours at 85 °C under continuous MPP tracking is not adequately supported by the presented data. Clear long-term MPPT results, with appropriate comparison to control devices and information on reproducibility should be provided.

Answer 5:

We thank the reviewer for this comment and have revised the claims accordingly. We further evaluated the impact of molecular glass interlayers on device stability using continuous maximum power point tracking (MPPT) measurements (Figure 9d). Compared with pristine devices, the molecular-glass-modified perovskite based devices exhibit higher and more stable power output under identical testing conditions, while the control devices show fast performance decay. The enhanced MPPT stability correlates with improved thermal stability of the molecular glass-modified perovskite films (Figure 4), reduced leakage currents (Figure 9c) and suppressed thermally induced degradation. These consistent perovskite film modification and device-level trends confirm that the sustained MPPT performance arises from effective interfacial thermal stabilization. Overall, these

results demonstrate that molecular glass electron-acceptor interlayers not only enhance device efficiency but also provide robust long-term operational stability with continuous MPPT serving as direct validation of the improved interfacial thermal robustness. We have added new discussion. Please see the line from 381 to 392.

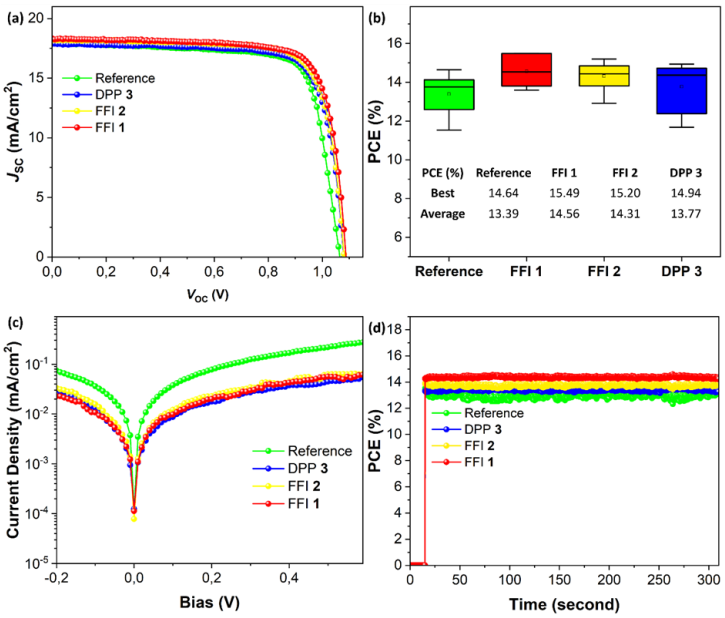

Figure 9. (a) The reverse scan *J–V* characteristics of perovskite solar cells fabricated without additives and with molecular glass additives FFI **1**, FFI **2**, and DPP **3**, (b) PCE comparison of pristine perovskite as reference, FFI **1**, FFI **2**, and DPP **3**, (c) comparison of dark *I-V* curve with and without molecular glass electron-acceptor compounds and (d) comparison MPPT curve perovskite with and without molecular glass electron-acceptor compounds.

Figure 9b confirms device reproducibility and the robustness of the stabilization effect across multiple devices.

We sincerely appreciate the reviewer's thoughtful comments and positive assessment of our manuscript. We are grateful for the opportunity to revise our paper and have carefully addressed all reviewer suggestions to improve the quality and clarity of the work. We believe that the revised version significantly enhances the manuscript and hope it will be valuable to the readers of Energy Technology.

Sincerely yours
Dr. Md. Shahiduzzaman
Corresponding author
Associate Professor
Kanazawa University, Japan

4

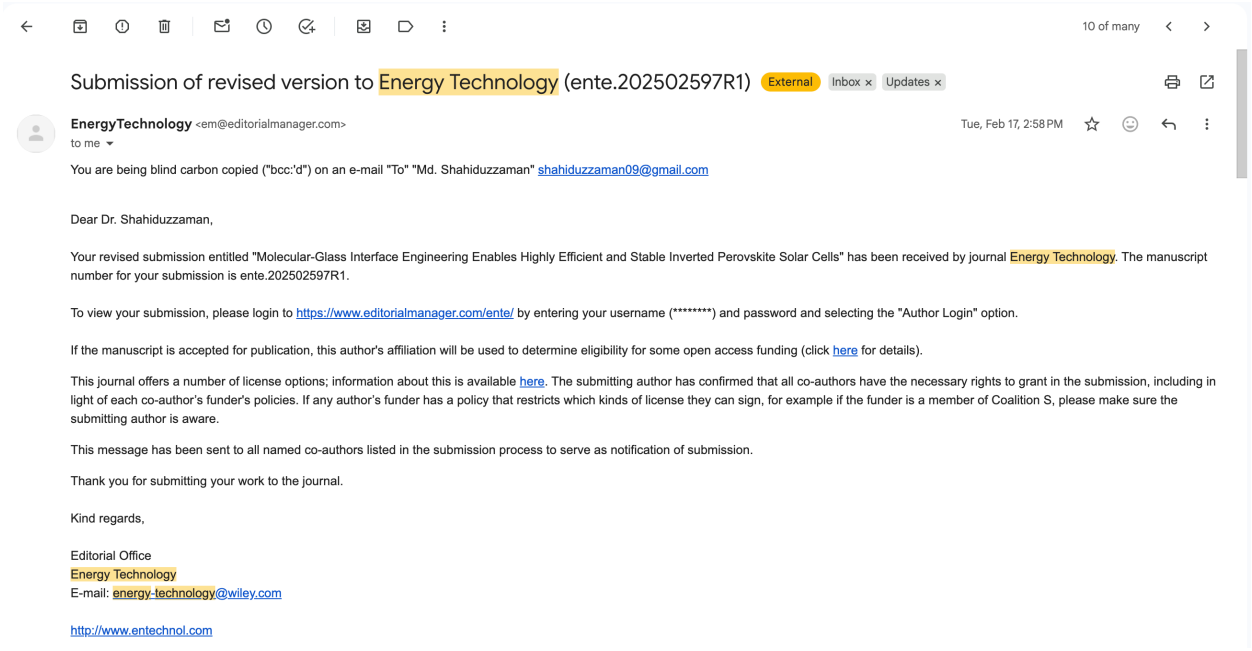

10 of many

Submission of revised version to Energy Technology (ente.202502597R1) External Inbox × Updates ×

EnergyTechnology <em@editorialmanager.com> Tue, Feb 17, 2:58 PM

to me

You are being blind carbon copied ("bcc:'d") on an e-mail "To" "Md. Shahiduzzaman" shahiduzzaman09@gmail.com

Dear Dr. Shahiduzzaman,

Your revised submission entitled "Molecular-Glass Interface Engineering Enables Highly Efficient and Stable Inverted Perovskite Solar Cells" has been received by journal Energy Technology. The manuscript number for your submission is ente.202502597R1.

To view your submission, please login to https://www.editorialmanager.com/ente/ by entering your username (********) and password and selecting the "Author Login" option.

If the manuscript is accepted for publication, this author's affiliation will be used to determine eligibility for some open access funding (click here for details).

This journal offers a number of license options; information about this is available here. The submitting author has confirmed that all co-authors have the necessary rights to grant in the submission, including in light of each co-author's funder's policies. If any author's funder has a policy that restricts which kinds of license they can sign, for example if the funder is a member of Coalition S, please make sure the submitting author is aware.

This message has been sent to all named co-authors listed in the submission process to serve as notification of submission.

Thank you for submitting your work to the journal.

Kind regards,

Editorial Office
Energy Technology
E-mail: energy-technology@wiley.com

http://www.entechnol.com

5

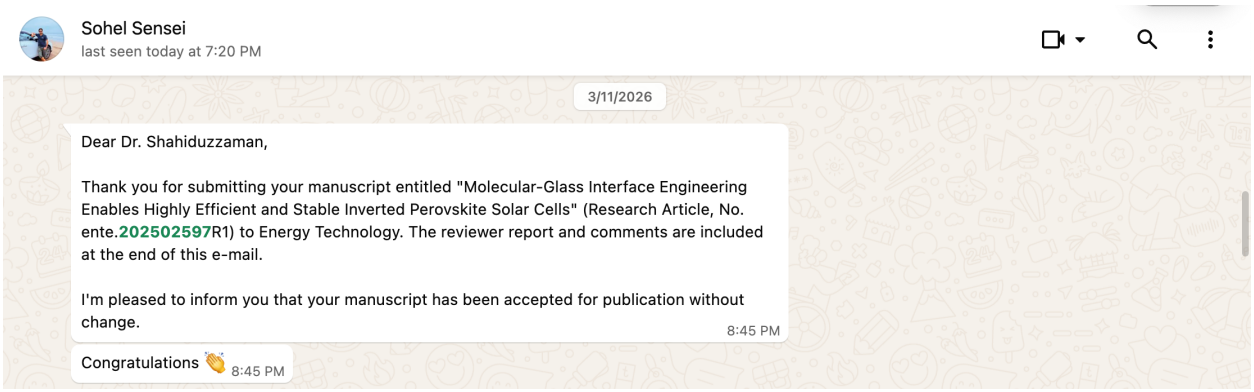
Sohel Sensei
last seen today at 7:20 PM
3/11/2026
Dear Dr. Shahiduzzaman,
Thank you for submitting your manuscript entitled "Molecular-Glass Interface Engineering Enables Highly Efficient and Stable Inverted Perovskite Solar Cells" (Research Article, No. ente.202502597R1) to Energy Technology. The reviewer report and comments are included at the end of this e-mail.
I'm pleased to inform you that your manuscript has been accepted for publication without change.
8:45 PM
Congratulations
8:45 PM

UNIVERSITAS TRISAKTI

Ersan Yudhapratama Muslih <ersan.ym@trisakti.ac.id>

Urgent_Fwd: Action: Proof of ENTE_EV_ENTE70451 for ENERGY TECHNOLOGY ready for review

1 message

Dr. M. Shahiduzzaman (Sohel) <shahiduzzaman09@gmail.com> Tue, Mar 24, 2026 at 8:23 AM
To: ersan muslih <ersanmuslih@gmail.com>, Ersan Muslih Yudhapratama Muslih <ersan.ym@trisakti.ac.id>

Salam Dr. Ersan

Can you please submit the review of your proof of your manuscript. Please complete it as soon as possible. Thank you.

Sohel

---------- Forwarded message ---------
From: **Wiley Online Proofing** <onlineproofing@wiley.com>
Date: Tue, Mar 24, 2026 at 1:14 AM
Subject: Action: Proof of ENTE_EV_ENTE70451 for ENERGY TECHNOLOGY ready for review
To: <shahiduzzaman09@gmail.com>

Review your proof

ENTE_EV_ENTE70451

Dear **Md. Shahiduzzaman,**

The proof of your **ENERGY TECHNOLOGY** article **Molecular Glass Interface Engineering Enables Highly Efficient and Stable Inverted Perovskite Solar Cells** is now available for review:

Edit Article

To review your article, please complete the following steps, ideally within 48 hours*, so we can publish your article as quickly as possible. We will not proceed with publication until we have heard back from you.

*We appreciate that there may be extenuating circumstances that make it difficult for you to review your proof within standard timeframes. If you require additional time, please reach out to us at (production-ente@wiley.com) to discuss alternatives.

1. Open your proof in the online proofing system using the button above.
2. Check the article for correctness and respond to all queries. For instructions on using the system, please see the "Help" menu in the upper right corner.
3. Please click **"Save"** before submitting your edits.
4. Submit your changes by clicking the "**Submit**" button in the proofing system.
5. If you have not already done so, please log in into Author Services (https://authorservices.wiley.com) and click on "My Dashboard". When you locate your article on the Dashboard, please click the button that says "Sign License"

WILEY

7

Redline PDF Help v.3.5.0

Article DOI : 10.1002/ente.202502 Author Proof

RESEARCH ARTICLE

Molecular Glass Interface Engineering Enables Highly Efficient and Stable Inverted Perovskite Solar Cells

Ersan Y. Muslih [1,2] | Neng Hani Handayani [3] | Masahiro Nakano [4] | Makoto Karakawa [3,4,5] | Mohammad Ismail Hossain [6] | Md. Akhtaruzzaman [7] | Jean-Michel Nunzi [5,8] | Olivier Lebel [9] | Tetsuya Taima [3,4,5] | Md. Shahiduzzaman [4,5]

[1]Environmental Engineering Department, ~~Faculty of Architecture Landscape and Environmental Engineering,~~ Faculty of Landscape Architecture and Environmental Technology, Universitas Trisakti, Jakarta, Indonesia

[2]Center of Excellent for Sustainable Energy and Materials, Universitas Trisakti, Jakarta, Indonesia

[3]Graduate School of Frontier Science Initiative, Kanazawa University, Kakuma, Kanazawa, Japan

[4]Graduate School of Natural Science and Technology, Kanazawa University, Kakuma, Kanazawa, Japan

[5]Nanomaterials Research Institute, Kanazawa University, Kakuma, Kanazawa, Japan

[6]Department of Electrical and Computer Engineering, University of California, Davis, California, USA

[7]Department of Chemical Engineering, Faculty of Engineering, Islamic University of Madinah, Madinah, Saudi Arabia

[8]Department of Physics, Engineering Physics and Astronomy, Queens University, Kingston, Ontario, Canada

[9]Department of Chemistry and Chemical Engineering, Royal Military College of Canada, Kingston, Ontario, Canada

Md. Akhtaruzzaman (akhtar.brces@gmail.com) |, Jean-Michel Nunzi (nunzijm@queensu.ca) |, Olivier Lebel (Olivier.Lebel@rmc.ca) |, Tetsuya Taima (taima@se.kanazawa-u.ac.jp) |, Shahiduzzaman (shahiduzzaman09@gmail.com),

Received Date: 17 November 2025 | **Revised Date:** 17 February 2026 | **Accepted Date:** 11 March 2026

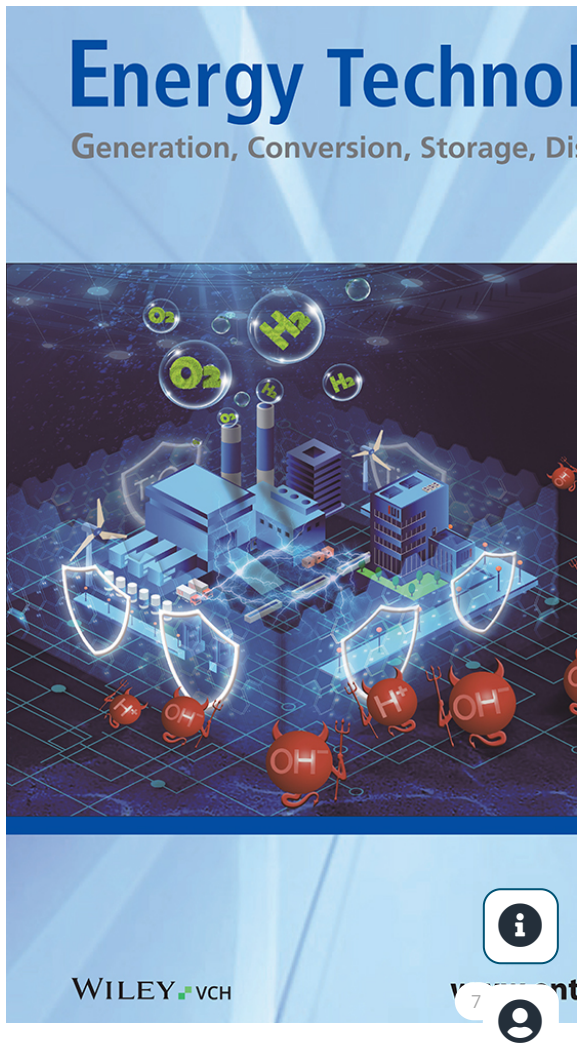

1 Proof Initiated
3/23/2026

2 Corresponding Author
Due date: 3/25/2026
Start date: 3/23/2026
End date: 3/24/2026

3 Proof Collator
Due date: 3/26/2026
Start date: 3/24/2026
End date: 3/27/2026

4 Completed

Abstract

Perovskite solar cells with inverted configuration (p–i–n) offer simple, low-temperature fabrication and high open-circuit voltage, but they are limited by poor thermal and moisture stability. Here, we introduce solution-processable amorphous molecular glass electron-acceptor interlayers, comprising two fused fluoranthene imide (FFI) derivatives and a diketopyrrolopyrrole (DPP) analog, which simultaneously enhance the efficiency and operational durability of $MAPbI_3$ p–i–n devices. These glassy films utilize strong π–π stacking, electron-withdrawing triazine and thiophene units, and inherent hydrophobicity to optimize energy-level alignment with PCBM, reduce ion migration, and prevent moisture ingress. The addition of FFI increases the champion power conversion efficiency (PCE) from 14.6% to 15.5% and raises the water contact angle from 77° to 108°. Under continuous maximum power point tracking at 85°C, FFI-modified cells retain over 90% of their initial PCE after 96 h, while control devices degrade within 48 h. X-ray diffraction and UV–Vis measurements confirm the sustained

durable perovskite photo

Author Proof

Graphical Abstract

First-principles calculations are used to investigate the structural stability, mechanical behavior, and optoelectronic and transport properties of Na_2LiMF_6 (M = Rh, Ir) double perovskites. Stability is confirmed through formation energy, elastic criteria, and tolerance factor analyses, while PBE–GGA and mBJ–GGA results indicate potential for optoelectronic and thermoelectric applications. The thermoelectric figure of merit increases with temperature, reaching 0.51 for Na_2LiRhF_6 and 0.31 for Na_2LiIrF_6 at 1200 K.

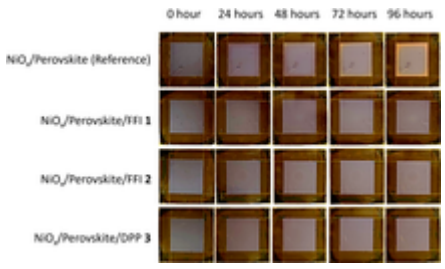

Keywords

energy-level alignment | inverted (p–i–n) perovskite solar cells | ion-migration suppression | molecular glass interlayers | operational stability

1 | Introduction

Perovskite solar cells (PSCs) have emerged as one of the most promising photovoltaic technologies due to their high-power conversion efficiency (PCE) exceeding 26% for n–i–p and p–i–n structure [1–6] yet with a low fabrication cost. However, their commercialization is hindered by stability issues and the need for efficient electron transport layers (ETLs) to optimize charge extraction. TiO_2 is widely used as the ETL in conventional n–i–p PSCs, but it is rarely employed in inverted p–i–n architectures because its high-temperature processing, interfacial mismatch, and photocatalytic activity are incompatible with perovskite films and it is not appropriate for hole-transport [7–11]. Thus, in p–i–n structure, ETLs, such as phenyl–C_{61}–butyric acid methyl ester (PCBM), are a common material due to low application temperature. In addition, PCBM molecules, whether blended into the bulk or added as a single layer as ETLs in devices, enhance electron transfer and can effectively reduce hysteresis [12–18]. However, the PCBM still has some shortcomings, such as it can still react with methylammonium iodide (MAI) or iodine ions, cannot repel H_2O molecules from outside, and even PCBM can penetrate into the perovskite grain boundaries, resulting in damage to the perovskite and a decrease in device performance [19–23]. Thus, interfacial modification with interlayer material helps protect the perovskite layer from ion migration and moisture-induced degradation, thereby improving long-term stability.

Interface modification has long been explored as a key strategy to improve both the efficiency and stability of PSCs. Among the reported approaches, ethylenediamine (EDA) has been used in Sn–Pb perovskites, where it successfully reduces trap states and enhances charge extraction [24]. Although ethylenediamine (EDA) has been reported to reduce interfacial trap states and facilitate charge extraction in perovskite-based devices, its practical applicability remains constrained by intrinsic material limitations, including high volatility, strong chemical reactivity, and well-documented corrosive and sensitizing properties, which raise concerns regarding handling safety and long-term interfacial stability

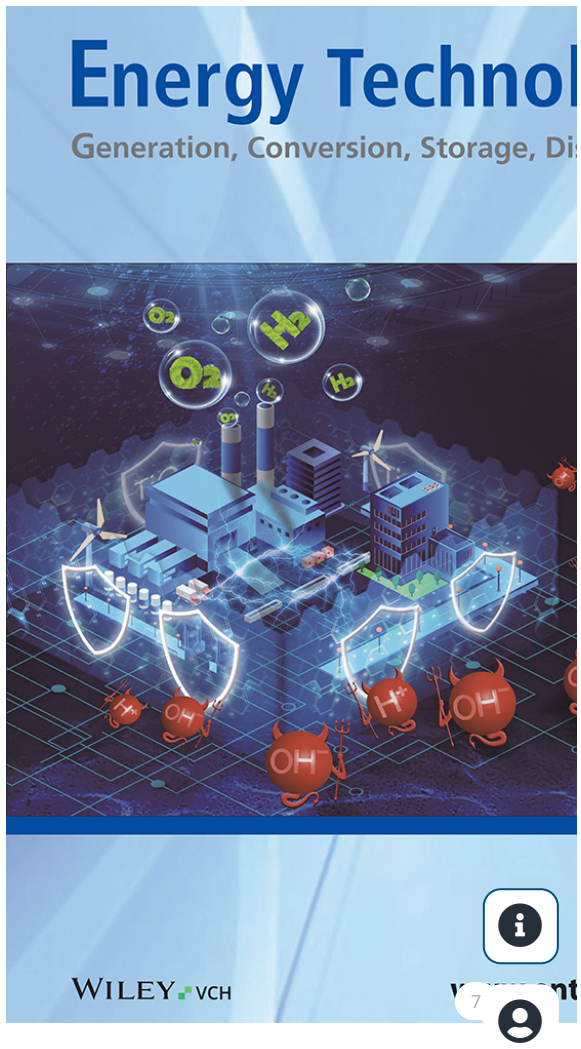

Unlike EDA, these materials [illegible] robust, nonvolatile, and capable of forming amorphous glassy interlayers that intimately coat the perovskite surface. Furthermore, they integrate defect passivation with additional functionalities, including hydrophobic protection, suppression of ion migration, and improved compatibility with PCBM. As a result, the molecular glass electron-acceptor compounds represent an evolutionary step in interfacial engineering, merging the defect passivation of earlier strategies, the multifunctionality of bifunctional ligands, and the robustness of glass-forming molecular systems. Collectively, these unique features establish them as a promising route toward achieving high-performance and durable PSCs. In the context of ligand-engineered PSCs, π–π interactions between aromatic moieties of multivalent ligands and the perovskite surface can enhance interfacial ordering and stability by promoting more uniform low-dimensional passivation layers, which in turn contribute to improved defect passivation and charge transport properties [29].

In this study, we present molecular glass electron-acceptor derivatives as potential interlayer materials between perovskite and PCBM in a p–i–n structure, and thoroughly examine their influence on device performance. These molecular glass derivatives are especially appealing due to their strong π-bonding, extended delocalization, and inherent hydrophobic properties. Additionally, they showcase excellent electron mobility, high photostability, and significant chemical tunability, making them versatile for interfacial engineering [30–39]. Beyond these inherent benefits, this research also investigates how the distinct electronic and chemical interactions of the molecular glass interlayers prevent the degradation of methylammonium lead iodide ($MAPbI_3$) into lead iodide (PbI_2). Consequently, adding these materials not only boosts the efficiency of PSCs but also greatly enhances their operational stability.

2 | Experimental Section

2.1 | Materials

AQ5 The fluorine-doped tin oxide (FTO) glass, with a thickness of 0.7 mm, resistivity of 9–10 Ω per square, and transmittance of 82-85%, was obtained from Nippon Sheet Glass Co., Ltd. (Tokyo, Japan). Acetone (C_3H_6O, 99.5% purity) and isopropanol (IPA, C_3H_8O, 99.5% purity) were sourced from Tokyo Chemical Industry Co., Ltd. (Tokyo, Japan). Lead iodide (PbI_2, 99.9% purity) was acquired from Tokyo Chemical Industry (Tokyo, Japan). *N*, *N*-dimethylformamide (DMF, 99.5% purity) were supplied by Wako Chemical (Tokyo, Japan). Dimethyl sulfoxide (DMSO, 99.5% purity), nickel nitrate pentahydrate ($Ni(NO_3)_2{\cdot}5H_2O$, 99.9% purity), methylammonium iodide (MAI, anhydrous, >99.9% purity), and ethanol (C_2H_6O, >99.9% purity) were obtained from Merck. Furthermore [6], -phenyl–C_{61}–butyric acid methyl ester (PCBM, 99.9%) and bathocuproine (BCP, 99.99%) were sourced from Sigma-Aldrich (Tokyo, Japan). Silver wire (Ag, 99.999% purity) was procured from Nilaco Corp. (Tokyo, Japan). Electron acceptors used were either previously published [31] or the complete synthetic details can be found in the Supporting Information.

2.2 | Device Fabrication

AQ6 The NiO_x thin film was made by dissolving 29.08 mg of $Ni(NO_3)_2{\cdot}5H_2O$ in 1000 µL ethanol 99.99% with constant stirring at 1000 rpm, then followed by filtering with PTFE 0.45 µ to filter some insoluble particles. The NiO_x thin film, serving as the hole transport layer, was deposited onto FTO-coated glass. The substrate was thoroughly cleaned using deionized water, acetone, and isopropyl alcohol, each undergoing 15 min of sonication. Afterward, it was dried with a nitrogen jet and subjected to

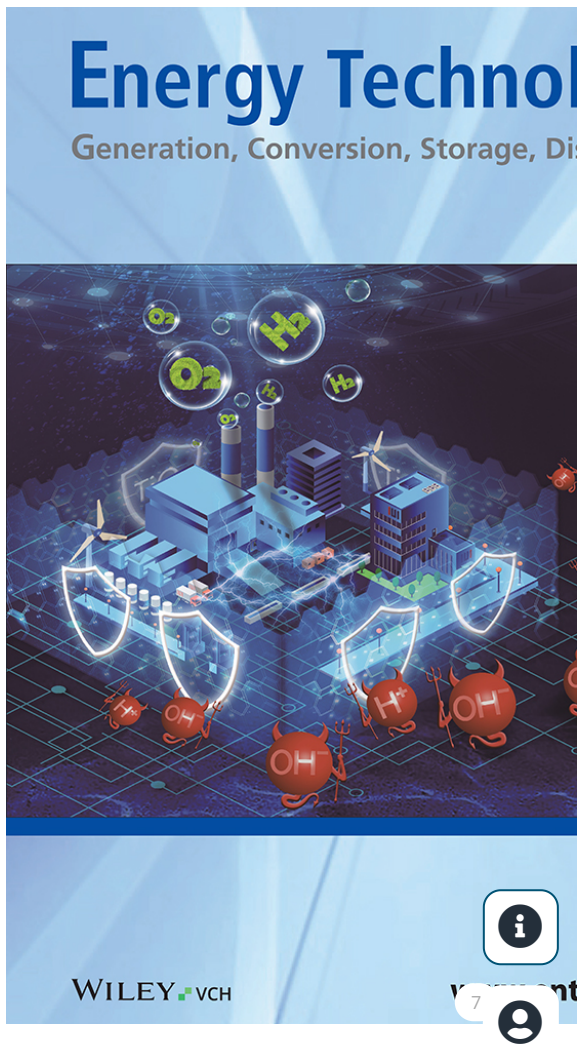

distributed using a spin-coa for 30 s, followed by annealing at 350°C for 3 h. The inverted PSCs were fabricated by depositing a precursor solution containing 1 M PbI_2 and 1 M MAI dissolved in 700 µL DMF and 300 µL DMSO, which had been stirred at 60°C for 12 h. This solution was spin coated onto a NiO_x thin film (acting as the hole transport layer) at 6000 rpm for 45 s, followed by annealing at 100°C for 15 min. Before deposition, the NiO_x layer underwent plasma cleaning in an ozone atmosphere for 10 min. Next, 20 mg/mL FFI or DPP compounds in chlorobenzene were deposited on perovskite using a spin coater at 2000 rpm for 30 s, and continued by drying at 105°C. Moreover, PCBM in chlorobenzene and 0.5 mg/mL BCP in ethanol were sequentially deposited via spin coating at 1500 rpm for 30 s and 4000 rpm for 30 s, respectively. Finally, a 100 nm silver (Ag) electrode was deposited through vacuum evaporation under a vacuum pressure of 4.5×10^{-4} Pa. The final device configuration was: glass/FTO/NiO_x/$MAPbI_3$/molecular glass electron-acceptor compounds/PCBM/BCP/Ag.

3 | Results and Discussion

Various small-molecule electron-acceptor derivatives can improve the performance of perovskite-based solar cells. Small-molecule electron acceptors are promising because they have multiple conjugated and delocalized double bonds, making them suitable as ETLs in PSCs. The materials developed by our group are even more unique due to their glass-forming properties, which allow them to be deposited from solution as amorphous thin films. In this study, two new glass-forming fused fluoranthene imide (FFI) derivatives **1** and **2**, along with previously reported as diketopyrrolopyrrole (DPP) derivative **3** (3,3′-Bis(6-hexyl-1,3-dihydro-2H-indol-2-one)−2,2′-bithiophene-5,5′-dicarboxamide) [31], were studied. The structure of those materials is shown in Figure 1.

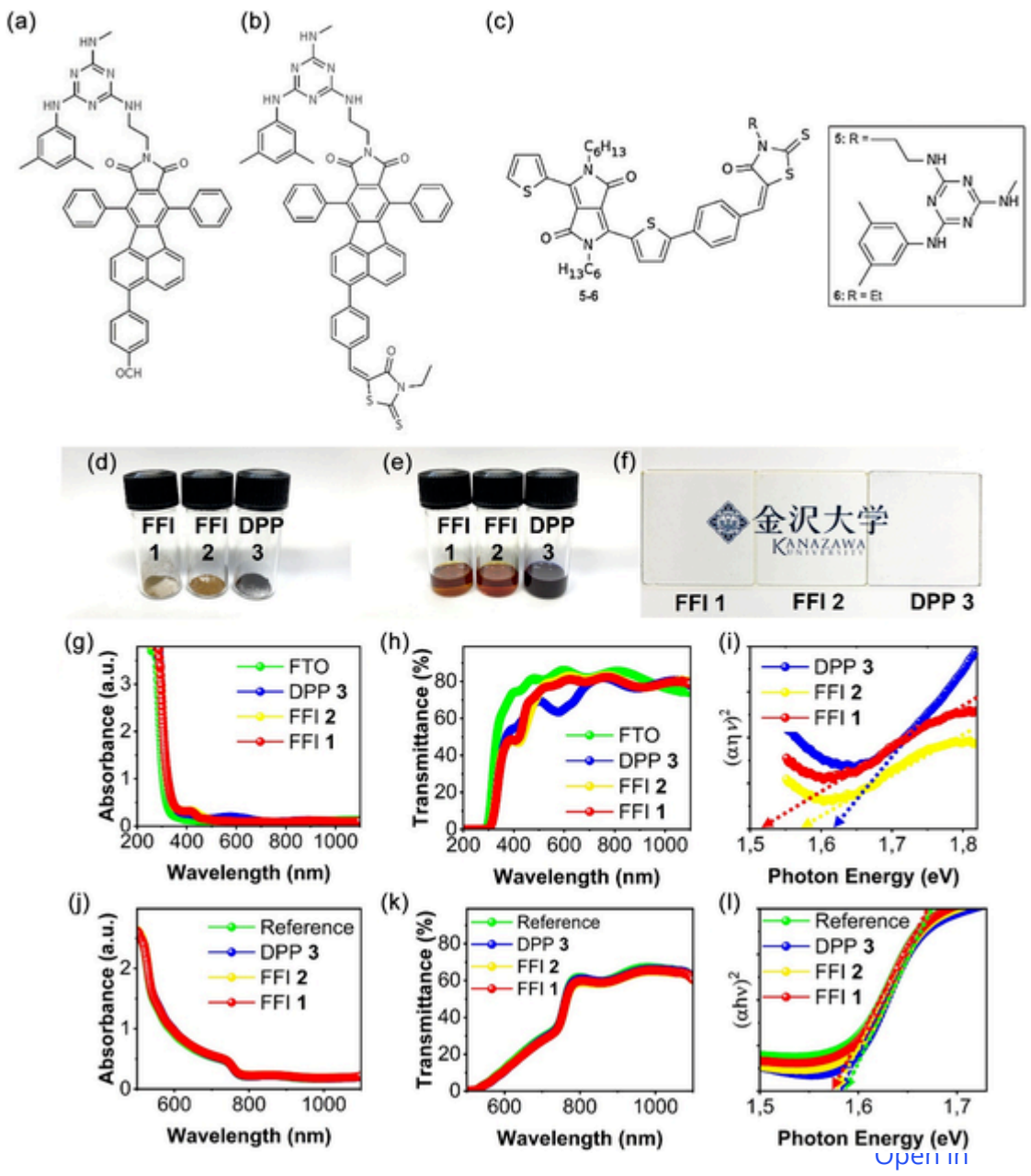

FIGURE 1.

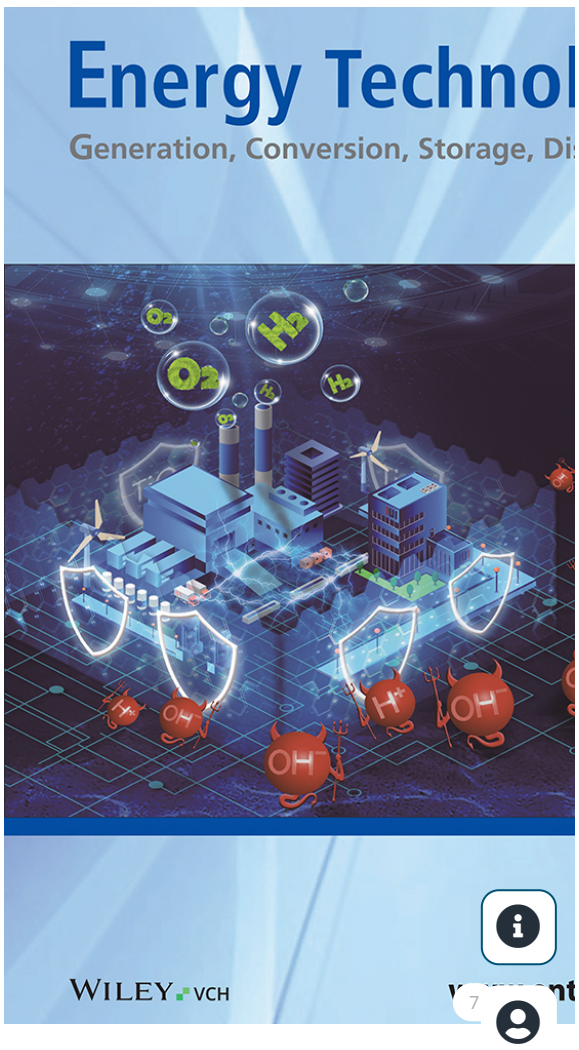

1 Proof Initiated
3/23/2026

2 Corresponding Author
Due date: 3/25/2026
Start date: 3/23/2026
End date: 3/24/2026

3 Proof Collator
Due date: 3/26/2026
Start date: 3/24/2026
End date: 3/27/2026

4 Completed

Open in figure viewer

and DPP **3** for their (g) abso ittance, and (i) Tauc plot, respectively. The optical properties of perovskite with FFI **1**, FFI **2**, and DPP **3** for its (j) absorbance, (k) transmittance, and (l) Tauc plot.

There are three ways that can be envisaged to introduce a mexylaminotriazine moiety on the FFI core: 1) on the imide side chain, 2) on one on the phenyl rings, or 3) on the fused naphthalene ring. Functionalizing the imide with the glass-inducing group enables a simple and divergent approach to screening different structures, even though it may not be optimal from a purely cost perspective. For this purpose, previously published amino glass **4** was converted to the corresponding maleimide **5** in 55% yield by condensation of the free –NH_2 group with maleic anhydride. This reaction was a half pathway to synthesis FFI **1** and FFI **2**. The reaction pathway is shown in Figure 2.

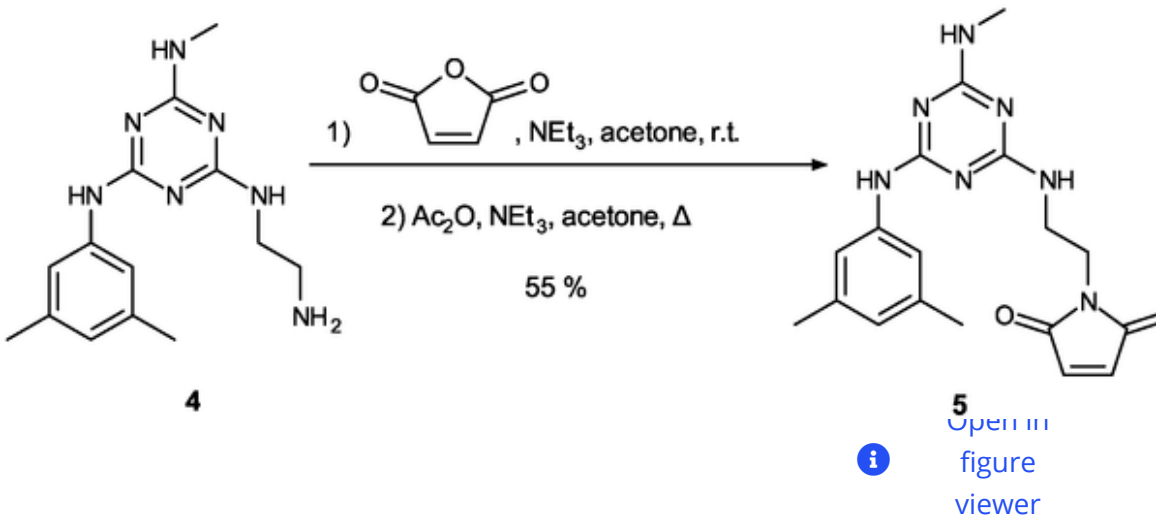

FIGURE 2.
Synthesis reaction of maleimide compound from amino glass compound.

Moreover, maleimide glass **5** was then condensed via a cycloaddition reaction with cyclopentadienone **6** in refluxing nitrobenzene to afford mexylaminotriazine-substituted FFI glass **7** in 33% yield. Glass **7** is substituted with a bromo group on its naphthalene ring system, enabling further substitution with electron-withdrawing substituents to enhance its electron-acceptor character. A 4-formylphenyl group was introduced via Suzuki coupling to yield aldehyde 5, which was then condensed with *N*-ethylrhodanine to afford rhodanine-substituted FFI **6**, in 67 and 95% yields, respectively. Compounds **4** and **5** could be conveniently purified by simple filtration on a short silica pad, while FFI **6** could be purified by reprecipitation. The successful synthesis of the intermediate and final glass-forming compounds was confirmed by ^{1}H, ^{13}C, and HSQC NMR spectroscopy, displaying the expected chemical shifts and correlations for all major protons and carbons as shown in **Figures S2–S13**. The complete synthesis reaction of FFI **1** and FFI **2** is shown in Figure 3.

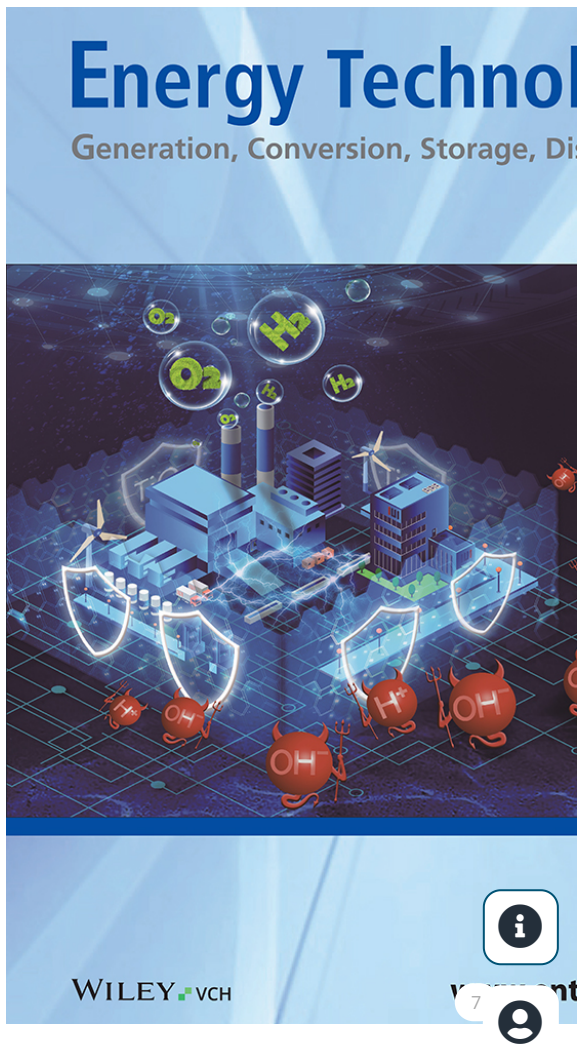

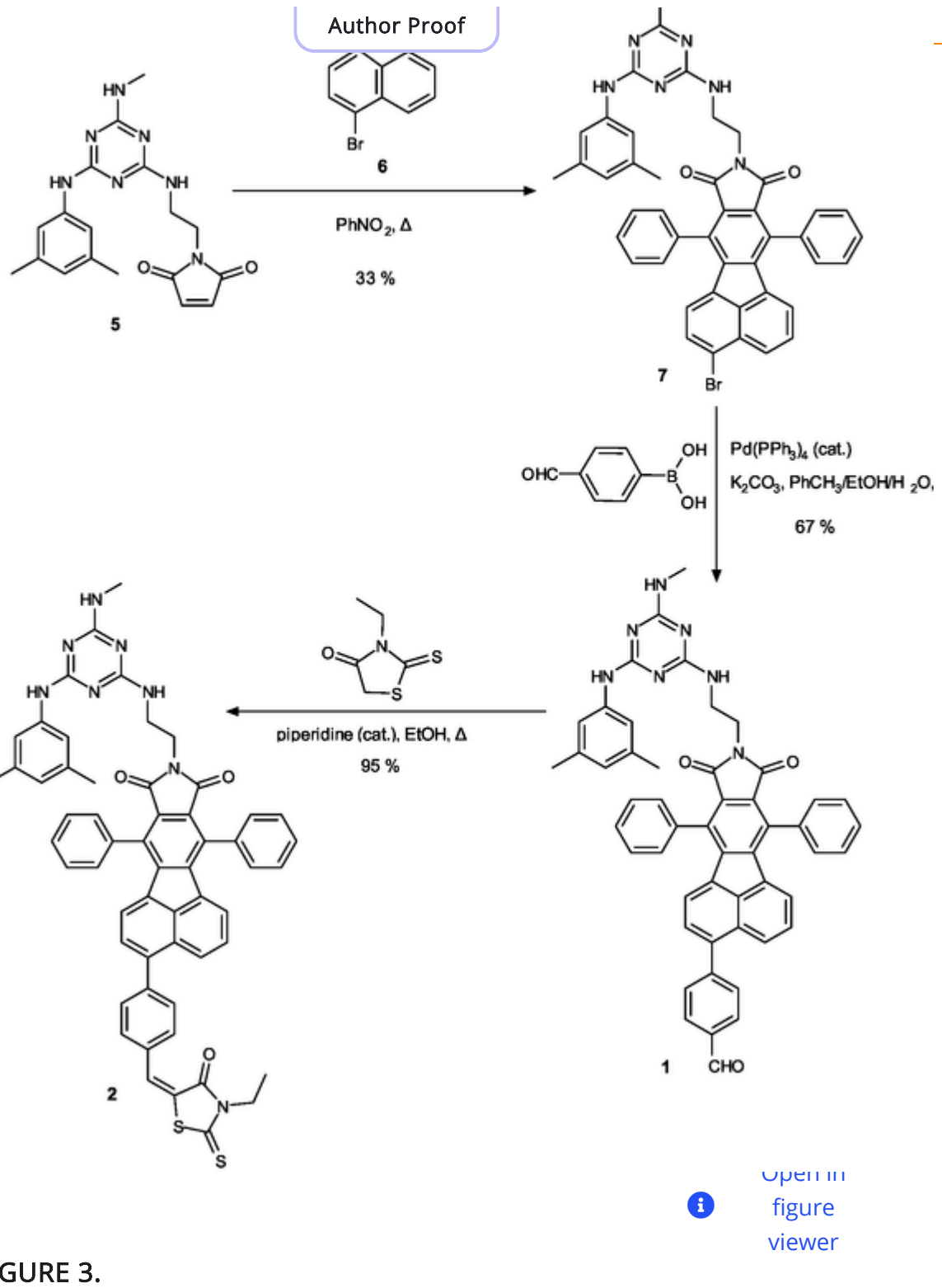

FIGURE 3.
Complete synthesis pathway of FFI **1** (shown as structure number 1) and FFI **2** (shown as structure number 2) from maleimide compound.

As with most mexylaminotriazine-substituted derivatives, precursor **5** expectedly showed glass formation with no recrystallization on heating or slow cooling, with a glass transition temperature (T_g) of 72°C, which is in the expected range for similar compounds. This glass-forming ability was successfully introduced in FFI derivatives **1–2** and **7**, which all showed T_g values ranging from 147 to 173°C, which are to be expected given the highly fused aromatic structures of the FFI moiety and the absence of long flexible chains. Again, no crystallization was observed for any of FFI glasses **1–2** and **7** under any conditions.

The UV–Vis spectrum data after depositing the molecular glass electron-acceptor compounds (FFI **1**, FFI **2**, and DPP **3**) on the perovskite layer reveal that the optical bandgap remains within the range from 1.57 to 1.58 eV, closely matching the reference perovskite layer. This stability in the bandgap suggests that the molecular glass electron-acceptor compounds do not significantly disrupt the perovskite's electronic structure. The absorption spectra of the molecular glass electron-acceptor compounds-modified perovskite layers closely follow the reference perovskite curve, indicating minimal alteration in optical properties and suggesting that these materials do not strongly absorb in the measured range. However, slight shifts or broadening at the absorption edge hint at potential interfacial interactions, such as charge transfer or dipole effects, which could influence carrier dynamics. The presence of these materials at the interface may modify charge transport and extraction without drastically affecting the intrinsic optical properties

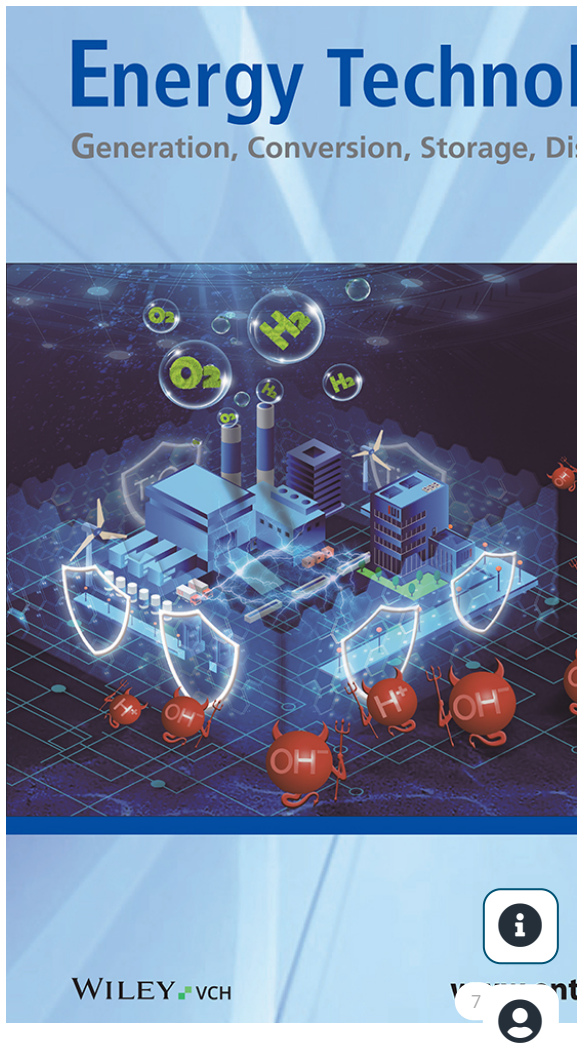

PSCs, optimizing charge tra Author Proof aintaining the fundamental absorption characteristics of the perovskite. The optical properties of perovskite modified by molecular glass electron-acceptor compounds are shown in Figure 1.

Furthermore, thermal stability test conducted over 96 h at 85 °C simultaneously provides crucial insights into the effectiveness of molecular glass electron-acceptor compounds in enhancing the stability of perovskite materials. As shown in Figure 4, the perovskite films incorporated with molecular glass electron-acceptor compounds exhibit remarkable stability, maintaining their structural integrity and visual uniformity throughout the test period. This suggests that molecular glass electron-acceptor compounds may act as protective layers, mitigating thermal degradation by preventing ion migration, inhibiting moisture penetration, or reducing defect formation at the interface. Typically, perovskite materials are prone to degradation under prolonged thermal stress, leading to phase segregation, oxidation, or decomposition. However, the preserved appearance of the molecular glass electron-acceptor modified films indicates that these materials enhance the perovskite's resistance to thermal-induced degradation, potentially extending the operational lifetime of PSCs. Further analysis, such as UV–Vis spectra and X-ray diffraction (XRD), could confirm whether the structural and electronic properties remain intact, reinforcing the role of molecular glass electron-acceptor compounds in stabilizing perovskite materials under thermal stress. These findings highlight the potential of molecular glass electron-acceptor compounds-functionalized interfaces in improving the long-term performance and commercial viability of perovskite-based photovoltaic devices. Figure 4 presents the UV–Vis spectra for the thermal stability of perovskite: (a) pristine perovskite as reference, perovskite with (b) FFI **1**, (c) FFI **2**, and (d) DPP **3**.

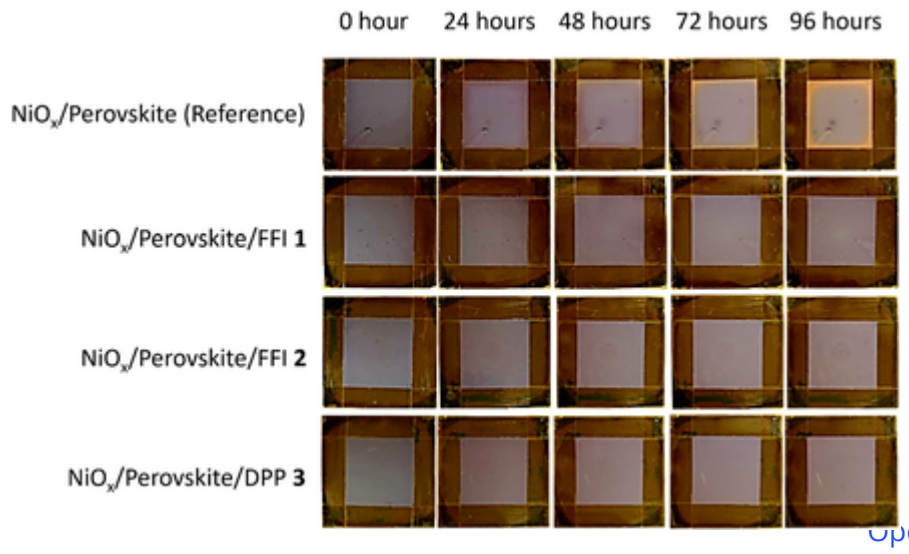

Open in figure viewer

FIGURE 4.
The appearance of perovskite with and without FFI **1**, **2**, and DPP **3** compounds on thermal stability test.

The complete set of UV–Vis spectra recorded during the 96-h thermal stability test is provided in the Supporting Information (**Figure S14**), which further confirms that the molecular glass-modified perovskite film retains its spectral profile and band edge positions, indicating suppressed thermal degradation compared to the pristine reference. The UV–Vis absorbance spectra shown in the image provide quantitative evidence supporting the thermal stability of perovskite materials incorporated with molecular glass electron-acceptor compounds over a 96-hour period at 85 °C. The absorbance curves at different time intervals (0 h, 24 h, 48 h, 72 h, and 96 h) show a gradual decrease in absorption intensity, a common characteristic of material degradation. However, the overall spectral shape and absorption edge remain relatively unchanged, indicating that the core optical properties of the

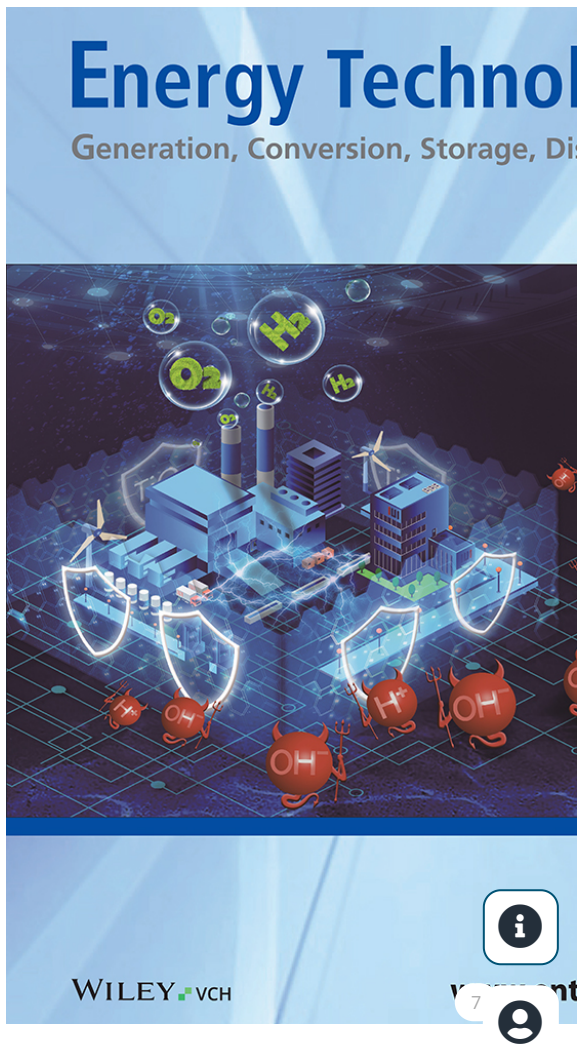

1 Proof Initiated
3/23/2026

2 Corresponding Author
Due date: 3/25/2026
Start date: 3/23/2026
End date: 3/24/2026

3 Proof Collator
Due date: 3/26/2026
Start date: 3/24/2026
End date: 3/27/2026

4 Completed

electron-acceptor compoun[illegible] maintaining the structural and electronic integrity of the perovskite films. The minor reduction in absorbance suggests that some degradation occurs over time, likely due to thermal stress, but the perovskite films with molecular glass electron-acceptor compounds remain optically active and structurally intact. This aligns with the hypothesis that the molecular glass electron-acceptor compounds act as protective interlayers, reducing ion migration and preventing decomposition pathways that typically lead to perovskite degradation. Furthermore, the stability observed in the UV–Vis spectra implies that the bandgap energy of the perovskite remains nearly unchanged, ensuring that charge carrier generation and transport properties are not significantly compromised over the 96-hour test. This is crucial for the long-term performance of PSCs, as maintaining high absorption efficiency directly correlates with sustained photovoltaic performance. **Figure S14** shows the impact of molecular glass electron-acceptor compounds on the perovskite layer under thermal stability test.

Moreover, Figure 5 illustrates the structural evolution and thermal stability of pristine and molecular glass-modified perovskite films during aging (0–96 hr), as revealed by XRD analysis. The XRD patterns compare pristine perovskite (a) with films incorporating molecular glass electron-acceptor additives FFI **1** (b), FFI **2** (c), and DPP **3** (d). The main diffraction peaks are marked with symbols, where α denotes the photoactive black α-phase perovskite, δ represents the undesired nonphotoactive δ-phase, and * indicates PbI_2, a typical degradation by-product. In the pristine film, the diffraction peak at $2\theta = 14.00°$, corresponding to the (100) plane, serves as the primary signature of the α-phase perovskite crystal structure, while the reflection at $2\theta = 20.11°$ is assigned to the (110) plane, representing a secondary but characteristic structural feature of halide perovskite [40–43]. Upon thermal exposure, the pristine sample exhibits pronounced structural degradation, as evidenced by the gradual attenuation of the α-phase reflections accompanied by the progressive emergence and intensification of the PbI_2 peak at 12.62°. Simultaneously, signatures of the δ-phase become more evident over time, indicating phase instability and partial transformation under thermal stress. This evolution reflects thermally activated iodide migration and defect-mediated decomposition, in which under-coordinated Pb^{2+} sites and halide vacancies act as nucleation centers for phase segregation toward PbI_2. The inset in Figure 5 highlights the evolution of the PbI_2 diffraction peak intensity over aging time, clearly demonstrating the accelerated degradation kinetics in the pristine film compared to the modified samples.

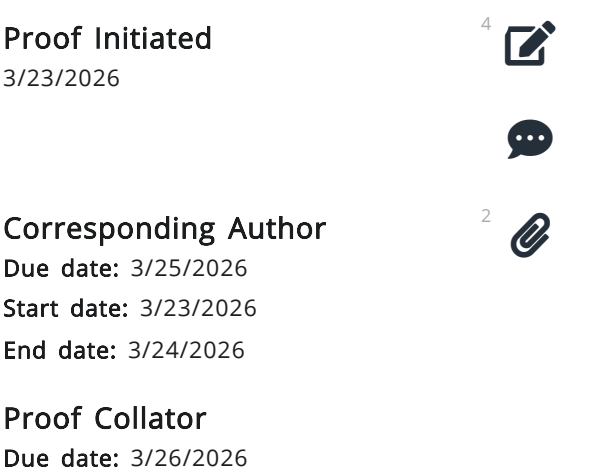

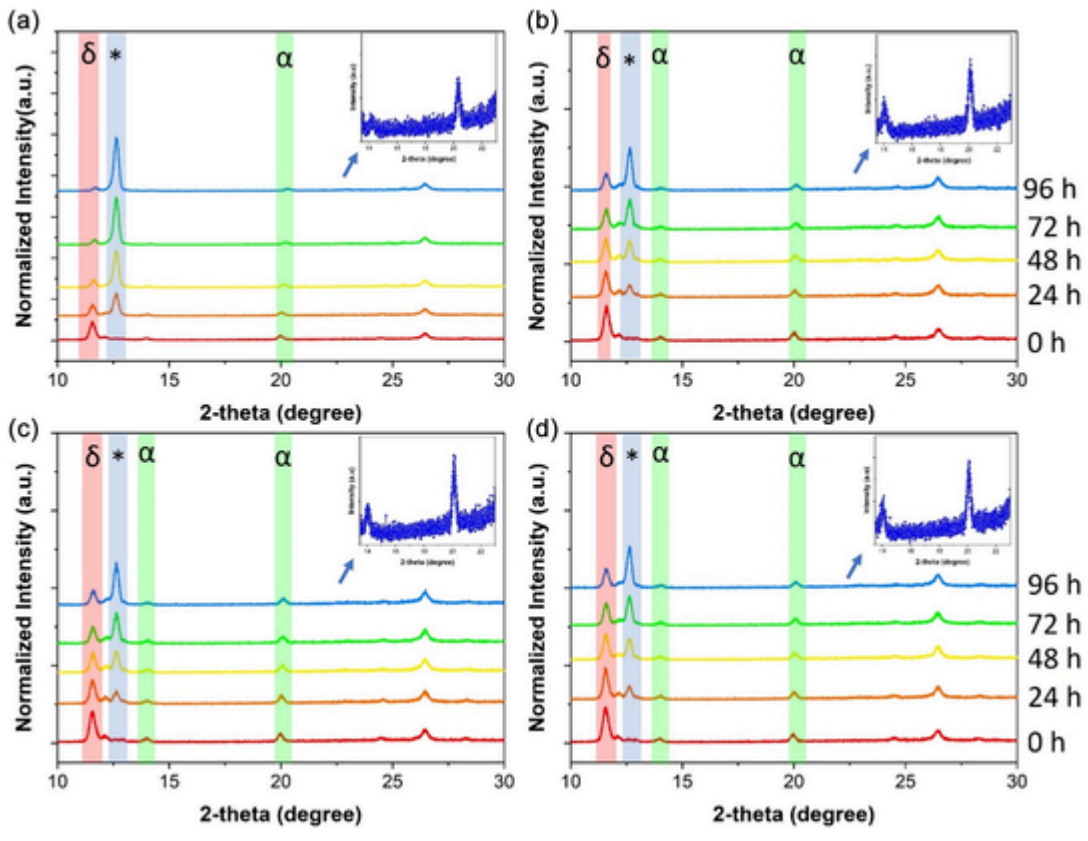

FIGURE 5:
Evolution of the crystal stru[illegible]tability of perovskite films during thermal aging at 85 °C for 0–96 h, analyzed by X-ray diffraction (XRD). (a) Pristine perovskite (reference), (b) perovskite with FFI 1, (c) perovskite with FFI 2, and (d) perovskite with DPP 3.~~(a) Thermal stability profiles of perovskite films with and without molecular glass additives measured at 85°C. The inset in (a) shows a magnified view of the initial degradation stage (0–20 hr). (b) Normalized PCE retention over time under continuous illumination. The inset in (b) presents the corresponding optical images of the films after 96 hr aging. PCE = Power conversion efficiency.~~

In contrast, the incorporation of molecular glass additives substantially mitigates these degradation pathways. The α-phase diffraction peaks remain comparatively stable in intensity over 96 hr, and the growth of the PbI_2 peak is markedly suppressed relative to the pristine film, demonstrating improved resistance to thermally induced phase segregation. The slower structural evolution observed in the modified films suggests that the molecular glass reduces defect density and stabilizes the perovskite lattice. Mechanistically, this enhancement can be attributed to several synergistic effects: coordination between molecular glass molecules and under-coordinated Pb^{2+} centers, which passivates structural defects; formation of an amorphous intergranular network that reinforces grain boundaries and limits lattice distortion; and suppression of halide ion migration, thereby inhibiting the autocatalytic decomposition process that typically accelerates degradation at elevated temperatures. Collectively, these effects kinetically and thermodynamically stabilize the perovskite structure, delaying the transition toward the PbI_2 phase and significantly enhancing the thermal robustness compared to the pristine counterpart.

The mechanism of perovskite decomposition has been extensively discussed by many researchers, with one of the main causes being the reaction between perovskite and water. Perovskite can also decompose into MAI and PbI_2. MAI can diffuse into the PCBM layer or evaporate as a gas, leaving behind yellow-colored PbI_2 as a degradation residue. Therefore, the structural degradation of perovskite can also be visually identified by changes in its color. If the perovskite layer begins to turn yellow, it indicates the formation of PbI_2, signaling the onset of decomposition. However, this phenomenon does not occur in perovskite layers that incorporate molecular glass electron-acceptor compounds. Molecular glass electron-acceptor compounds are well known for their extensive π-conjugated systems, which enable strong π–π interactions, resulting in enhanced electron delocalization and mobility. This feature is crucial for ETLs, as it enables efficient charge extraction from the perovskite layer to the electrode, minimizing charge recombination. The molecular glass electron-acceptor compounds have highly planar structures, promoting tight molecular packing and superior charge transport properties compared to conventional organic ETLs like PCBM.

Moreover, when molecular glass electron-acceptor compounds are introduced, a perovskite–molecular glass electron-acceptor compounds interface layer forms, exhibiting hydrophobic properties. This hydrophobicity arises from the extensive conjugated and delocalized bonds within the molecular glass electron-acceptor compounds, which effectively repel atmospheric water molecules and hydrophilic MAI molecules. This hydrophobicity can be seen from the contact angle of molecular glass electron-acceptor compounds on the perovskite surface in Figure 6, which increased from 77° in pristine perovskite to 107.0°, 108.4°, and 108.3° for FFI **1**, FFI **2**, and DPP **3**, respectively. As a result, MAI does not diffuse into the PCBM layer or escape into the

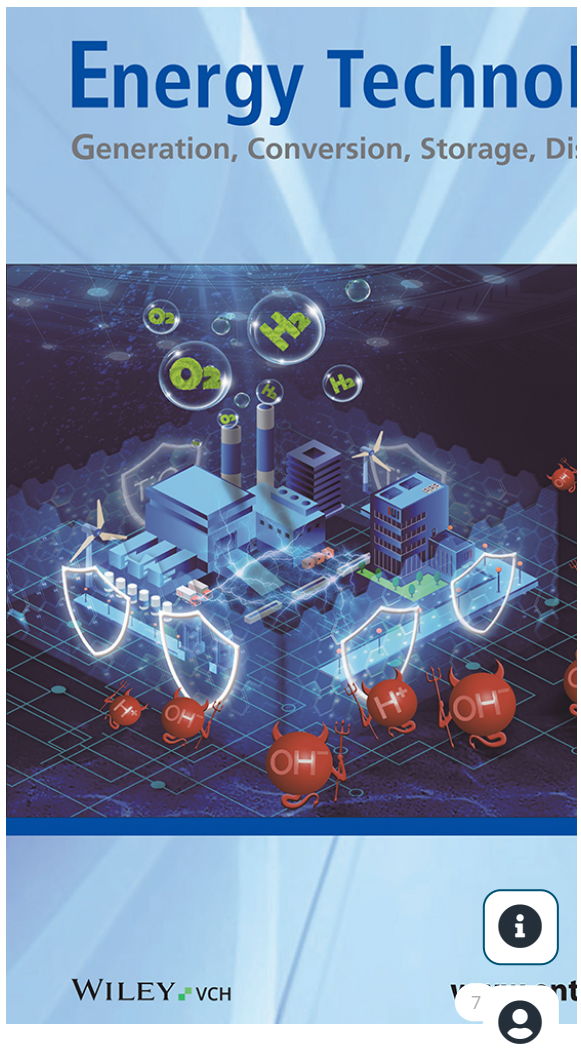

are shown in Figure 6.

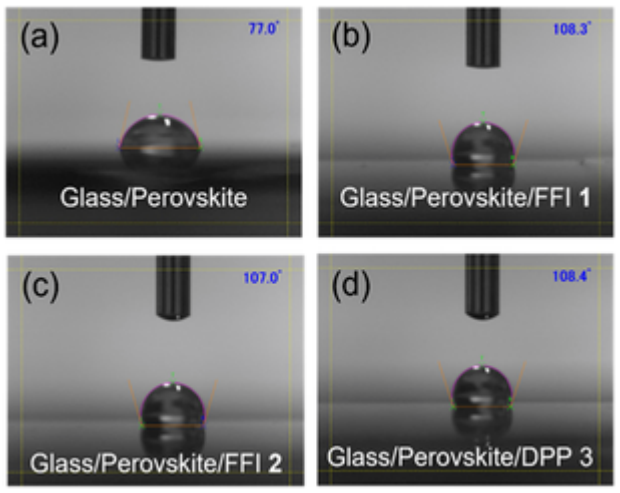

FIGURE 6.
Contact angle test of perovskite with and without FFI **1**, FFI **2**, and DPP **3** compounds after 96 h stability test.

Moreover, this hydrophobic perovskite–molecular glass electron-acceptor compounds interface enhances the compatibility between the perovskite and PCBM layers. This is because molecular glass electron-acceptor compounds share structural similarities with PCBM, including delocalized conjugated bonds and hydrophobicity, ensuring better interfacial contact. Additionally, molecular glass electron-acceptor compounds can still interact well with perovskite due to the triazine and thiophene functional groups, which can bind with the perovskite structure, further enhancing its stability. The decomposition and stability mechanisms are shown in Figure 7.

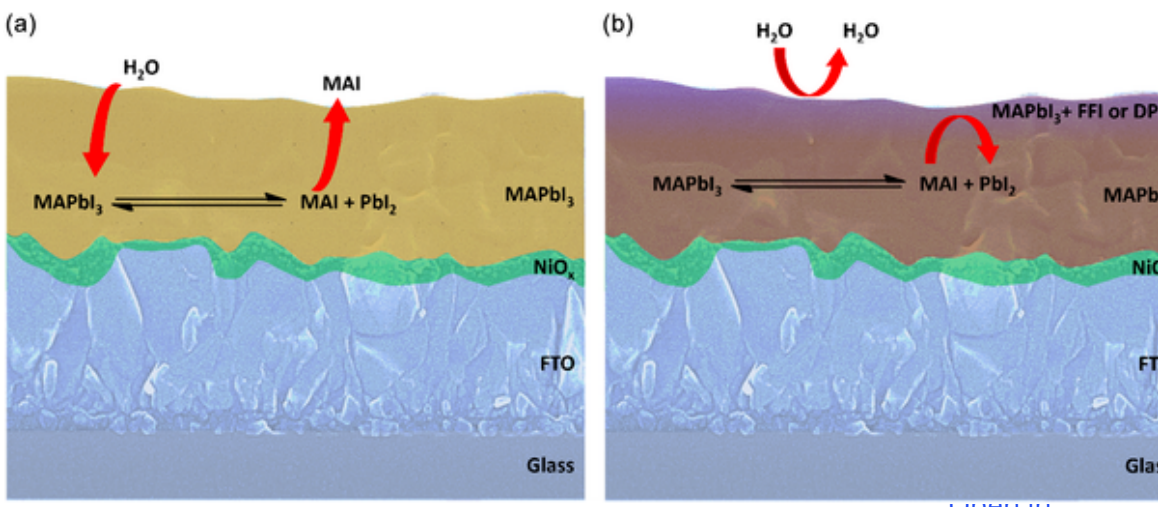

FIGURE 7.
(a) The illustration of perovskite degradation on thermal stability test and (b) stability mechanism of perovskite due to added by molecular glass electron-acceptor compounds. The structure for thermal stability test was glass/FTO/NiO_x/$MAPbI_3$/molecular glass electron-acceptor compounds.

The hydrophobicity of molecular glass electron-acceptor compounds, resulting from conjugated and delocalized double bonds, enables them to repel external water molecules from the perovskite. This effectively suppresses perovskite degradation into MAI and PbI_2 while preventing MAI from reacting with PCBM and blocking PCBM diffusion into perovskite grain boundaries. Additionally, the molecular glass electron-acceptor compounds interlayer facilitates smooth electron migration from perovskite to PCBM, minimizing ion migration. These combined effects significantly enhance the long-term thermal stability of the perovskite film when molecular glass electron-acceptor compounds are used as ETLs.

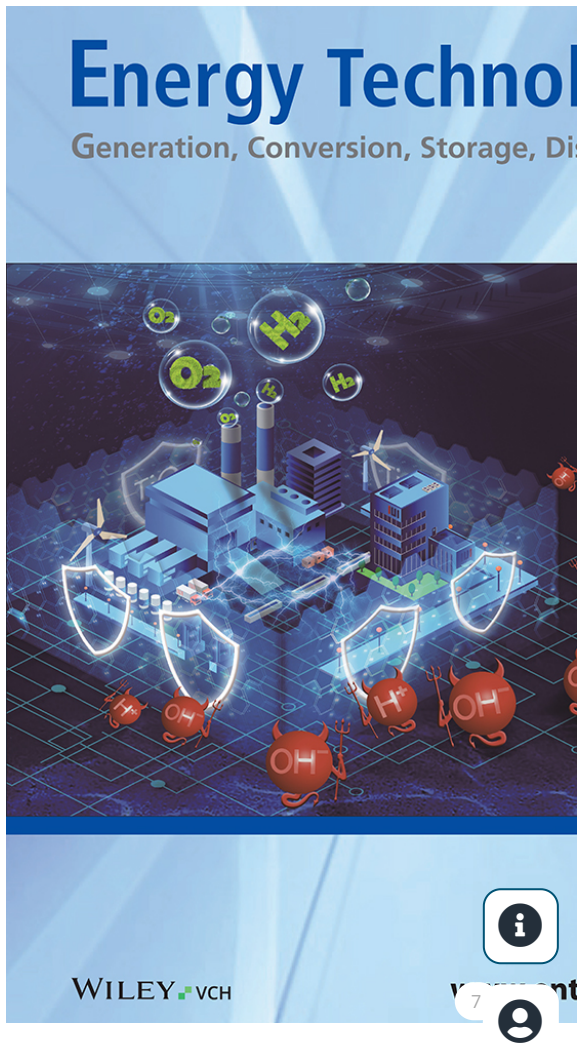

perovskite surface and pen Author Proof boundaries, forming a protective hydrophobic layer. This encapsulation effect prevents moisture infiltration and thermal-induced degradation, thus improving the perovskite's resilience to environmental stressors. Consequently, the presence of molecular glass electron-acceptor compounds contributes to enhanced hydrophobicity and thermal stability, making this approach promising. Figure 8 shows the SEM image of pristine perovskite as a reference and perovskite added with molecular glass electron-acceptor compounds.

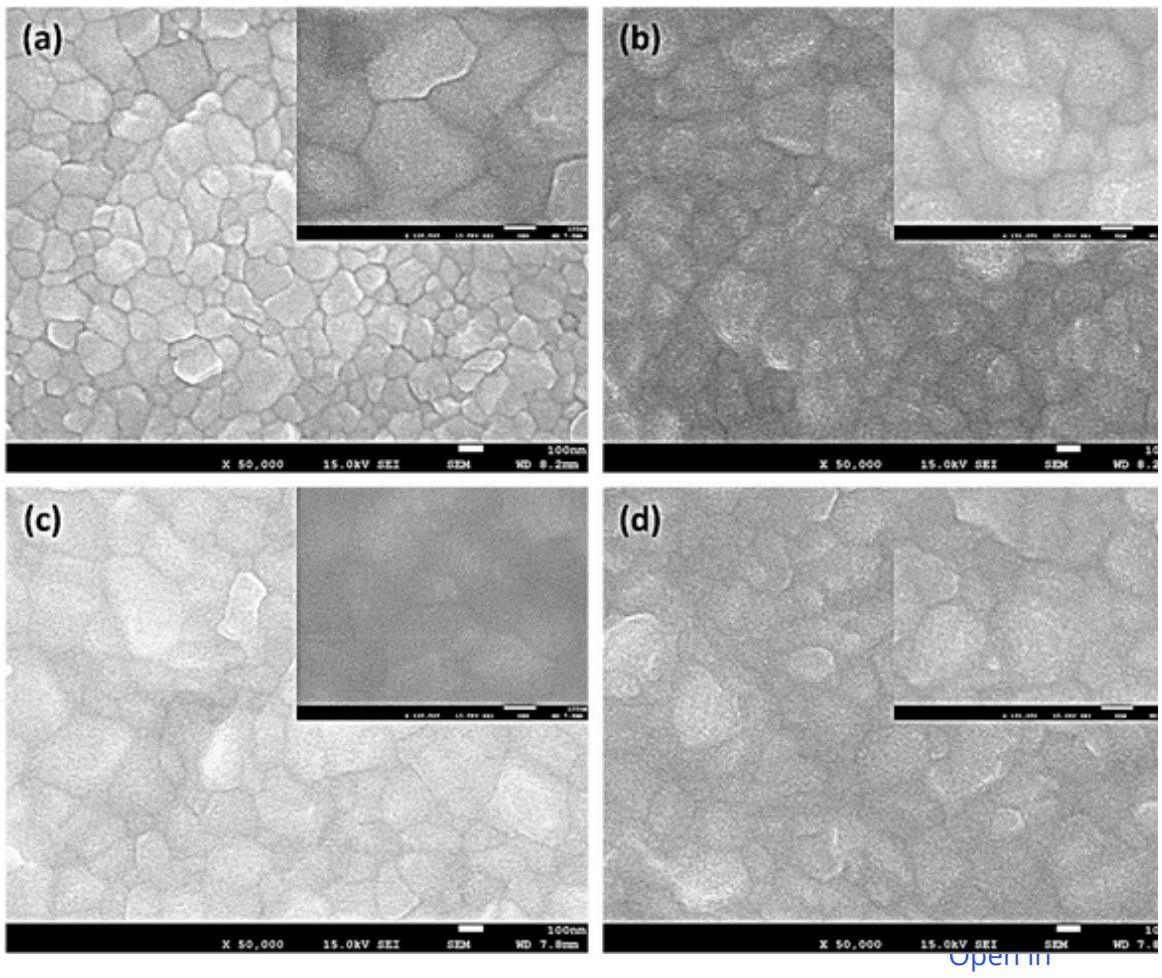

FIGURE 8.
SEM image of (a) pristine perovskite as a reference, perovskite with (b) FFI **1**, (c) FFI **2**, and (d) DPP **3**. SEM = Scanning electron microscopy.

Figure 9a presents the reverse scan *J–V* characteristics of PSCs fabricated without additives and with molecular glass electron-acceptor compounds. The plots clearly demonstrate variations in *Jsc* and *Voc* depending on the incorporated molecular glass. The reference device yields a *Jsc* of 17.86 mA/cm [2] and a *Voc* of 1.06 V, values typical of pristine PSCs. Upon the addition of molecular glass, the *J–V* behavior is distinctly modified. Among all samples, the device with FFI **1** achieves the highest *Jsc*, suggesting more efficient charge generation and extraction. This improvement can be attributed to enhanced film quality, higher crystallinity, and suppression of trap-assisted recombination. FFI **2** and DPP **3** also produce stable *J–V* curves with comparable *Voc* to the reference, although their *Jsc* values remain slightly lower than that of FFI **1**. In particular, the performance of DPP **3** is close to the reference, reflecting modest gains in current density but improved device stabilization. These findings confirm that molecular glass additives enhance overall photovoltaic performance, with FFI **1** providing the most pronounced effect.

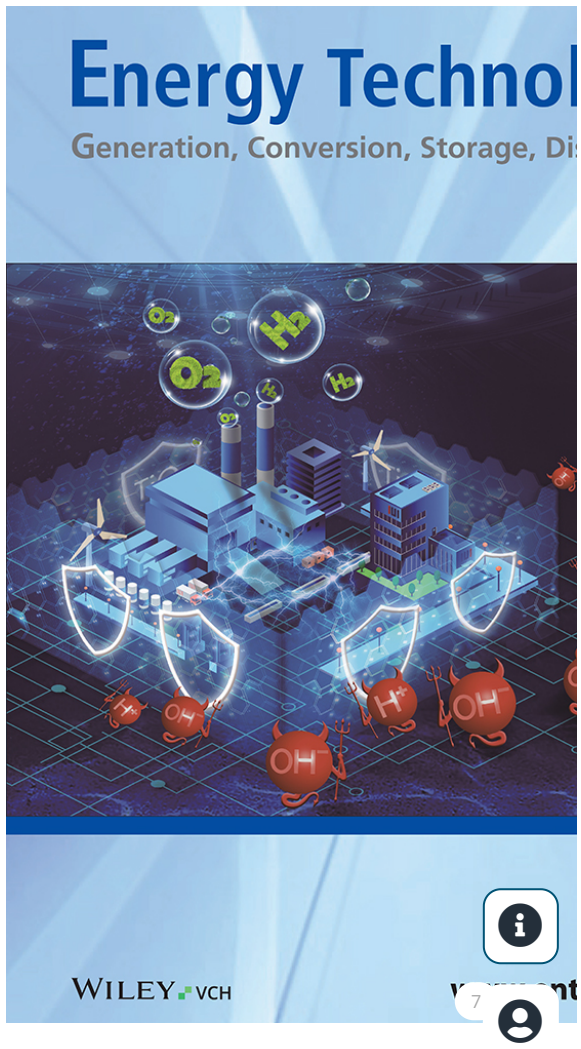

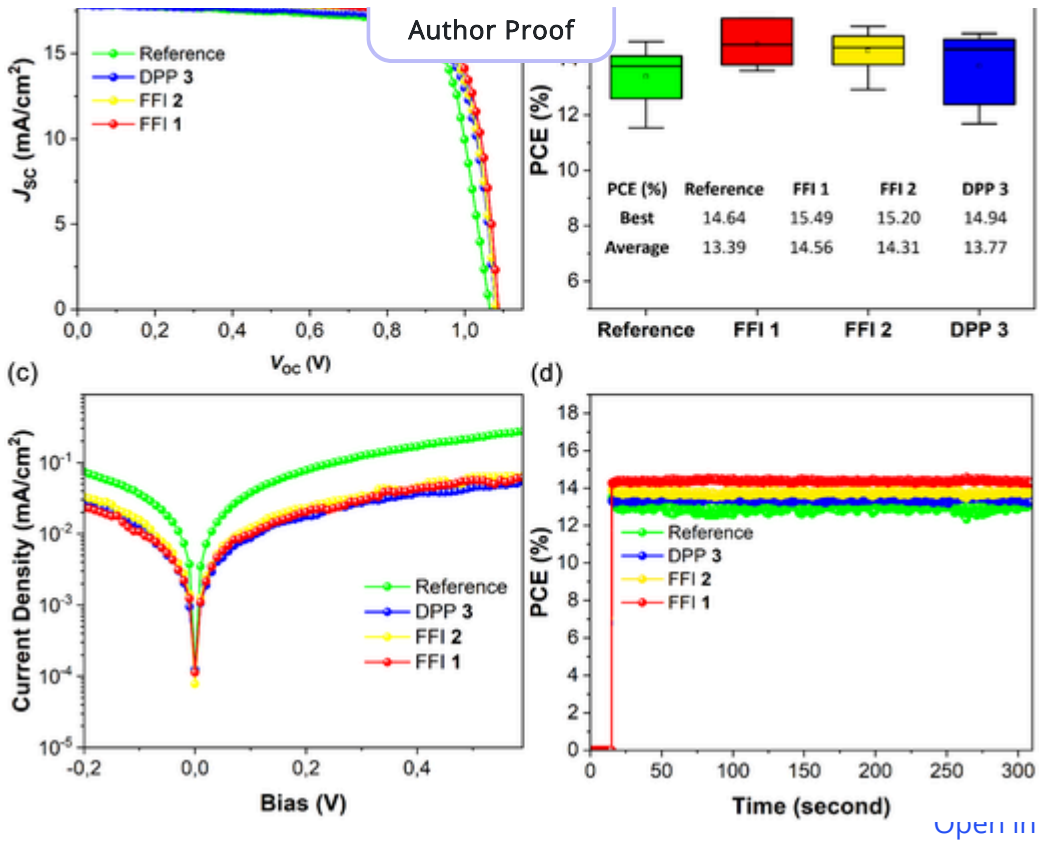

FIGURE 9.
(a) The reverse scan *J–V* characteristics of PSCs fabricated without additives and with molecular glass additives FFI **1**, FFI **2**, and DPP **3**, (b) PCE comparison of pristine perovskite as reference, FFI **1**, FFI **2**, and DPP **3**, (c) comparison of dark *I–V* curve with and without molecular glass electron-acceptor compounds and (d) comparison MPPT curve perovskite with and without molecular glass electron-acceptor compounds. PCE = Power conversion efficiency.

The *J–V* data further reveal improvements across all key photovoltaic parameter (PCE, *Jsc*, *Voc*, and FF) when molecular glass-based interlayers are introduced. Notably, FFI **2** records the highest *Jsc* of 18.50 mA/cm [2], demonstrating superior charge collection. Meanwhile, *Voc* increases slightly to 1.08 V for both FFI **1** and FFI **2**, indicating better energy-level alignment between the perovskite absorber and ETL. The fill factor remains stable across devices, showing that the additives do not introduce significant series resistance or additional recombination losses. The reduced hysteresis between forward and reverse scans further suggests the suppression of ion migration and improved interfacial charge transport. These effects are corroborated in **Figure S15**, which compares *J–V* curves at maximum PCE for devices with and without molecular glass. The molecular design of these additives plays a crucial role in enhancing performance. Triazine moieties provide strong electron-withdrawing properties, resulting in favorable energy-level alignment with the perovskite conduction band and facilitating efficient electron injection. Thiophene units, on the other hand, contribute molecular flexibility and improved charge transfer, which enhance overall transport characteristics [44, 45]. As a result, the modified devices achieve higher PCEs than the reference: FFI **1** reaches 15.49% (reverse scan), followed by FFI **2** at 15.20% and DPP **3** at 14.94%. These improvements demonstrate the ability of molecular glass electron-acceptor compounds to enhance charge extraction and mitigate recombination losses, as shown in Figure 9b. Further insights are obtained from the dark *I–V* characteristics. Molecular glass-based devices exhibit significantly reduced leakage currents compared to the reference, confirming better charge-blocking capability and suppression of recombination at the interfaces. The presence of triazine and thiophene groups within the interlayer enhances charge mobility and energy-level alignment, facilitating efficient electron transfer from the perovskite to PCBM. Lower dark current indicates effective suppression of ion

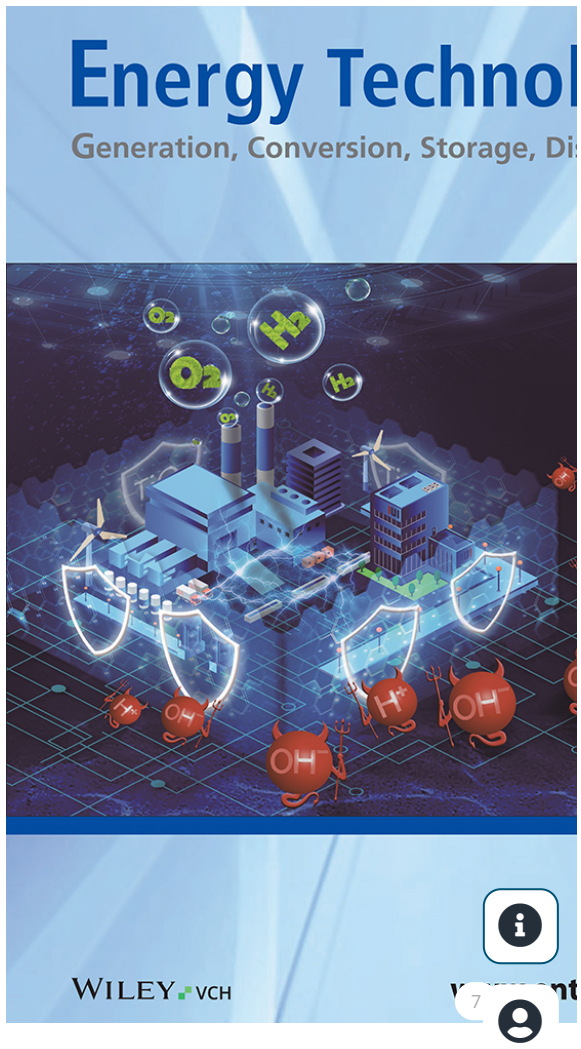

in Figure 9c.

We further evaluated the impact of molecular glass interlayers on device stability using continuous maximum power point tracking (MPPT) measurements (Figure 9d). Compared with pristine devices, the molecular glass-modified perovskite-based devices exhibit higher and more stable power output under identical testing conditions, while the control devices show fast performance decay. The enhanced MPPT stability correlates with improved thermal stability of the molecular glass-modified perovskite films (Figure 4), reduced leakage currents (Figure 9c), and suppressed thermally induced degradation. These consistent perovskite film modification and device-level trends confirm that the sustained MPPT performance arises from effective interfacial thermal stabilization. Overall, these results demonstrate that molecular glass electron-acceptor interlayers not only enhance device efficiency but also provide robust long-term operational stability with continuous MPPT serving as direct validation of the improved interfacial thermal robustness.

Moreover, the data clearly indicate the significant enhancement in device performance when molecular glass electron-acceptor compounds are introduced as an interfacial layer between perovskite and PCBM. The reference device, which employs only PCBM as the ETL, exhibits a moderate PCE, with relatively lower *Jsc* and *Voc*, likely due to suboptimal charge extraction and increased recombination at the interface. In contrast, PSCs modified with molecular glass electron-acceptor compounds show a substantial improvement in all key photovoltaic parameters. This improvement is attributed to the strong π–π stacking interactions in the molecular glass electron-acceptor compounds, which enhance charge transport, and the presence of triazine and thiophene functionalities, which facilitate better energy level alignment and suppress interfacial defects. Among the FFI **1**, FFI **2**, and DPP **3**-based interlayers, FFI **2** demonstrates the highest PCE, indicating its superior ability to improve charge extraction and stability. The higher *Jsc* observed in FFI **2**-modified devices suggests more efficient electron collection, while the increase in *Voc* implies reduced nonradiative recombination losses. Moreover, the FF is significantly improved, signifying reduced series resistance and enhanced charge transfer dynamics. The DPP **3** and FFI **1** interlayers also exhibit improved performance compared to the reference, though slightly lower than FFI **2**, reinforcing the beneficial effects of FFI **1**, FFI **2**, and DPP **3** compounds. Table 1 provides a detailed comparison of the photovoltaic parameters such as PCE, *Jsc*, *Voc*, and FF for the reference device and PSCs integrated with various molecular glass compound interlayers.

TABLE 1. Comparison of *J–V* curve with and without molecular glass electron-acceptor compounds at best PCE.

Device	Scan direction	*Jsc* (mA/cm^2)	*Voc* (V)	FF	PCE (%)
Reference	Forward	17.54	1.06	0.75	14.01
	Reverse	17.95	1.06	0.77	14.64
FFI 1	Forward	18.44	1.08	0.76	15.17
	Reverse	18.32	1.08	0.78	15.49
FFI 2	Forward	18.50	1.07	0.76	15.06
	Reverse	18.20	1.08	0.77	15.20

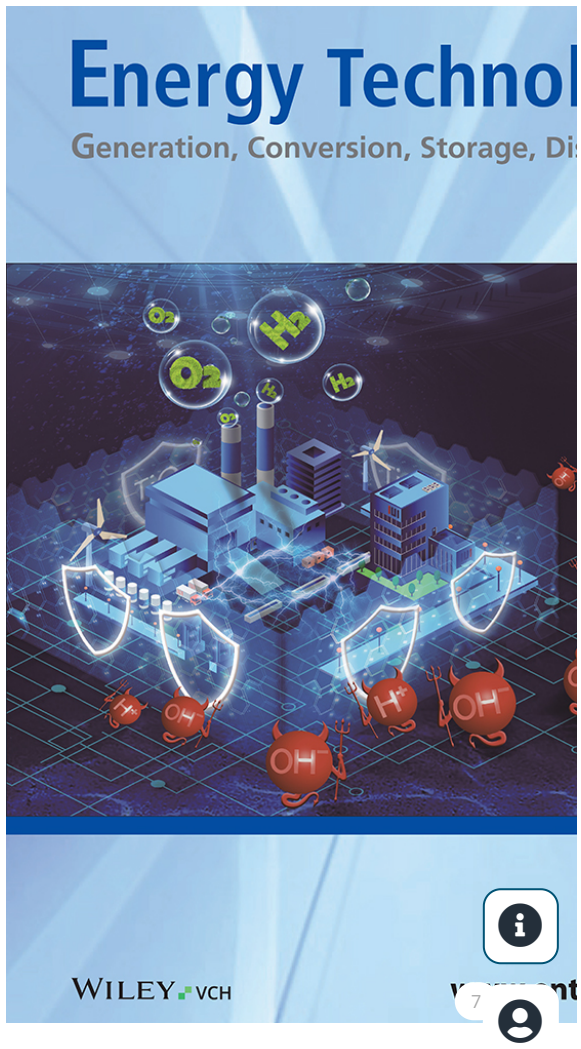

DPP 3	Forward	Author Proof	1.07	0.76	14.61
	Reverse	17.87	1.07	0.78	14.94

4 | Conclusions

AQ7

This work demonstrates that glass-forming molecular electron-acceptor compounds are highly effective interfacial layers for inverted $MAPbI_3$-based PSCs. Molecular glass-modified perovskite films exhibit excellent thermal stability at 85°C for 96 hr, as confirmed by XRD, SEM, and UV–Vis analysis. Mechanistic insights reveal that strong π–π stacking, electron-withdrawing triazine/thiophene units, and amorphous glass-like morphology collectively enhance interfacial robustness. The increase in water contact angle from 77° to over 108° further indicates the formation of durable hydrophobic barriers that suppress MAI diffusion and PbI_2 formation. This intrinsic materials stability translates directly into enhanced device performance, including reduced leakage currents and improved efficiency and stability. Consequently, MPPT measurements demonstrate sustained and stable power output, confirming that the improved operational stability arises from the robust thermal and interfacial stabilization imparted by the molecular glass interlayers.

Supporting Information

Additional supporting information can be found online in the Supporting Information section. **Supporting Fig. 1:** HOMO and LUMO orbitals of FFI glasses 1 and 2 as calculated by DFT (B3LYP/6,31G(d,p)). The mexylaminotriazine group was omitted from the calculations since it contributes minimally to the electronics of the FFI chromophore. (a) HOMO orbital of glass 1, (b) LUMO orbital of glass 1, (c) HOMO orbital of glass 2, (d) LUMO orbital of glass 2.

Acknowledgments

This study was partially supported by a Grant-in-Aid for Scientific Research (grant number 24K17769). Research at Queens was also supported by the the Natural Sciences and Engineering Research Council of Canada (RGPIN-2020−07016). The authors also extend their appreciation to the research support by the Deanship of Graduate Studies and Scientific Research at the Islamic University of Madinah, Saudi Arabia.

Supporting Information

Supplementary Material

1. ente70451-sup-0001-SuppData-S1.pdf

References

1. J. Zhou, L. Tan, Y. Liu, et al., “Highly Efficient and Stable Perovskite Solar Cells via a Multifunctional Hole Transporting Material,” *Efficient and Stable Perovskite Solar Cells via a Multifunctional Hole Transporting Material. Joule* 8, no. 6 (2024): 1691–1706, https://doi.org/10.1016/J.JOULE.2024.02.019.

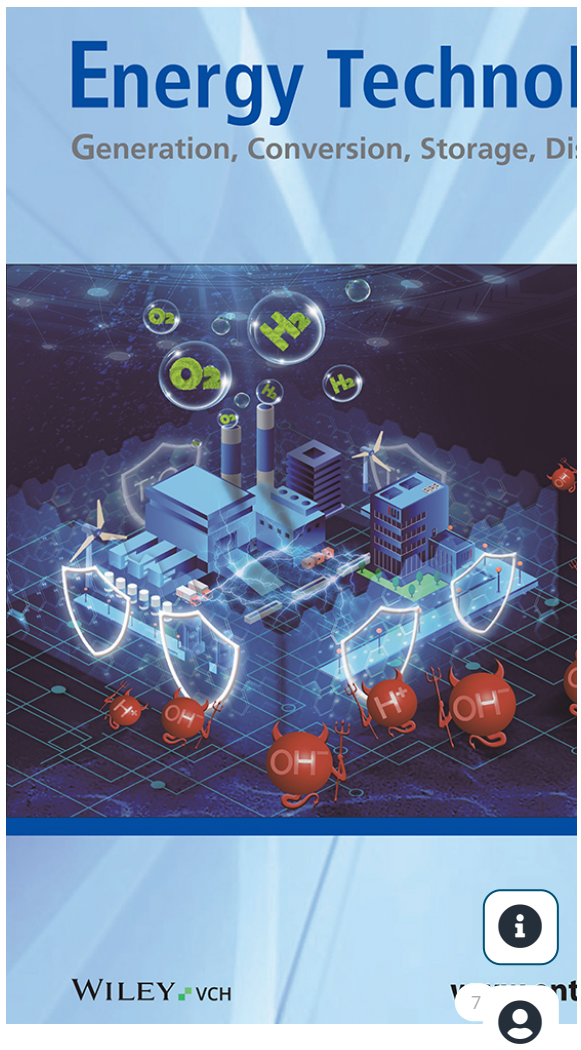

York, N.Y.) 384, 6692 (19[illegible]93, https://doi.org/10.1126/SC[illegible]4/SUPPL_FILE/SCIENCE.ADM9474_SM.PDF.

3. R. Azmi, D. S. Utomo, B. Vishal, et al., "Double-Side 2D/3D Heterojunctions for Inverted Perovskite Solar Cells," *Nature* 628, 8006 (2024): 93–98, https://doi.org/10.1038/s41586-024-07189-3.

4. R. Azmi, E. Ugur, A. Seitkhan, et al., "Damp Heat–Stable Perovskite Solar Cells with Tailored-Dimensionality 2D/3D Heterojunctions," *Science (New York, N.Y.)* 376, no. 6588 (2022): 73–77, https://doi.org/10.1126/science.abm5784.

5. X. Liu, B. Zheng, L. Shi, et al., "Perovskite Solar Cells Based on Spiro-OMeTAD Stabilized with an Alkylthiol Additive," *Nature Photonics* 17, no. 1 (2023): 96–105, https://doi.org/10.1038/s41566-022-01111-x.

6. S. Gong, G. Qu, Y. Qiao, et al., "A Hot Carrier Perovskite Solar Cell with Efficiency Exceeding 27% Enabled by Ultrafast Hot Hole Transfer with Phthalocyanine Derivatives," *Energy & Environmental Science* 17, no. 14 (2024): 5080–5090, https://doi.org/10.1039/D4EE01839G.

7. V. J. Garcia, C. M. Pelicano, and H. Yanagi, "Low Temperature-Processed ZnO Nanorods-TiO2 Nanoparticles Composite as Electron Transporting Layer for Perovskite Solar Cells," *Thin Solid Films* 662 (2018): 70–75, https://doi.org/10.1016/J.TSF.2018.07.039.

8. A. A. Qureshi, H. M. A. Javed, S. Javed, et al., "Incorporation of Zr-Doped TiO2 Nanoparticles in Electron Transport Layer for Efficient Planar Perovskite Solar Cells," *Surfaces and Interfaces* 25 (2021): 101299, https://doi.org/10.1016/J.SURFIN.2021.101299.

9. L. K. Ono, E. J. Juarez-Perez, and Y. Qi, "Progress on Perovskite Materials and Solar Cells with Mixed Cations and Halide Anions," *ACS Applied Materials and Interfaces. American Chemical Society September* 9 (2017): 30197–30246, https://doi.org/10.1021/acsami.7b06001.

10. P. Chen, Y. Xiao, S. Li, et al., "The Promise and Challenges of Inverted Perovskite Solar Cells," *Chemical Reviews* 124, no. 19 (2024): 10623–10700, https://doi.org/10.1021/acs.chemrev.4c00073.

11. M. Gantumur, M. Shahiduzzaman, M. I. Hossain, et al., "Revolutionizing Light Capture: A Comprehensive Review of Back-Contact Perovskite Solar Cell Architectures," *T. Revolutionizing Light Capture: A Comprehensive Review of Back-Contact Perovskite Solar Cell Architectures. Materials Today. Elsevier B.V.* (2025), https://doi.org/10.1016/j.mattod.2025.08.017.

12. Y. Zhong, M. Hufnagel, M. Thelakkat, C. Li, and S. Huettner, "Role of PCBM in the Suppression of Hysteresis in Perovskite Solar Cells," *Advanced Functional Materials* 30 (2020): 23, https://doi.org/10.1002/adfm.201908920.

13. F. Zhang, W. Shi, J. Luo, et al., "Isomer-Pure Bis-PCBM-Assisted Crystal Engineering of Perovskite Solar Cells Showing Excellent Efficiency and

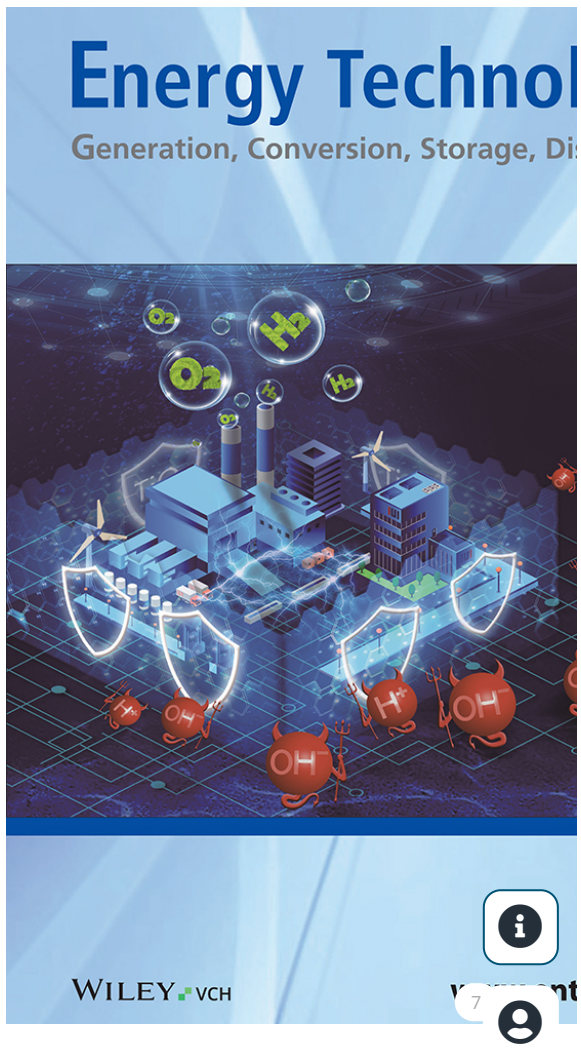

14. Y. Shao, Z. Xiao, C. Bi, Y. Yuan, and J. Huang, "Origin and Elimination of Photocurrent Hysteresis by Fullerene Passivation in CH3NH3PbI3 Planar Heterojunction Solar Cells," *Nature Communications* 5 (2014), https://doi.org/10.1038/ncomms6784.

15. E. Bi, H. Chen, F. Xie, et al., "Diffusion Engineering of Ions and Charge Carriers for Stable Efficient Perovskite Solar Cells," *Nature Communications* 8 (2017), https://doi.org/10.1038/ncomms15330.

16. K. Wojciechowski, S. D. Stranks, A. Abate, et al., "Modification for Highly Efficient Organic-Inorganic Perovskite Solar Cells," *ACS Nano* 8, no. 12 (2014): 12701–12709, https://doi.org/10.1021/NN505723H/SUPPL_FILE/NN505723H_SI_001.PDF.

17. E. Y. Muslih, Md Shahiduzzaman, Md Akhtaruzzaman, et al., "Reproducible Perovskite Solar Cells Using a Simple Solvent-Mediated Sol–gel Synthesized NiOx Hole Transport Layer," *Applied Physics Express* 15, no. 1 (2022): 015504, https://doi.org/10.35848/1882-0786/ac435d.

18. M. J. M. Marques, W. Lin, T. Taima, S. Umezu, and M. Shahiduzzaman, *Unleashing the Potential of Industry Viable Roll-to-Roll Compatible Technologies for Perovskite Solar Cells: Challenges and Prospects. Materials Today*. Elsevier B.V, September 1, 2024). 112–141, https://doi.org/10.1016/j.mattod.2024.06.013

19. L. Shen, P. Song, K. Jiang, et al., "Ultrathin Polymer Membrane for Improved Hole Extraction and Ion Blocking in Perovskite Solar Cells," *Nature Communications* 15, no. 1 (2024), https://doi.org/10.1038/s41467-024-55329-0.

20. C. Gong, H. Li, H. Wang, et al., "Coordination-Induced n-Doping of PCBM for Stable and Efficient Inverted Perovskite Solar Cells," *Nature Communications* 15, no. 1 (2024), https://doi.org/10.1038/s41467-024-49395-7.

21. Z. Shen, Q. Han, X. Luo, et al., "Efficient and Stable Perovskite Solar Cells with Regulated Depletion Region," *Nature Photonics* 18, no. 5 (2024): 450–457, https://doi.org/10.1038/s41566-024-01383-5.

22. S. You, F. T. Eickemeyer, J. Gao, et al., "Hole-Shuttle Molecule for Improved Interfacial Energy Level Alignment and Defect Passivation in Perovskite Solar Cells," *Nature Energy* 8, no. 5 (2023): 515–525, https://doi.org/10.1038/s41560-023-01249-0.

23. Md Shahiduzzaman, E. Y. Muslih, A. K. M. Hasan, et al., "The Benefits of Ionic Liquids for the Fabrication of Efficient and Stable Perovskite Photovoltaics," *Chemical Engineering Journal* 411 (2021): 128461, https://doi.org/https://doi.org/10.1016/j.cej.2021.128461.

24. G. Kapil, T. Bessho, T. Maekawa, et al., "Tin-Lead Perovskite Fabricated via Ethylenediamine Interlayer Guides to the Solar Cell Efficiency of 21.74%," *Advanced Energy Materials* 11, no. 25 (2021): 2101069, https://doi.org/https://doi.org/10.1002/aenm.202101069.

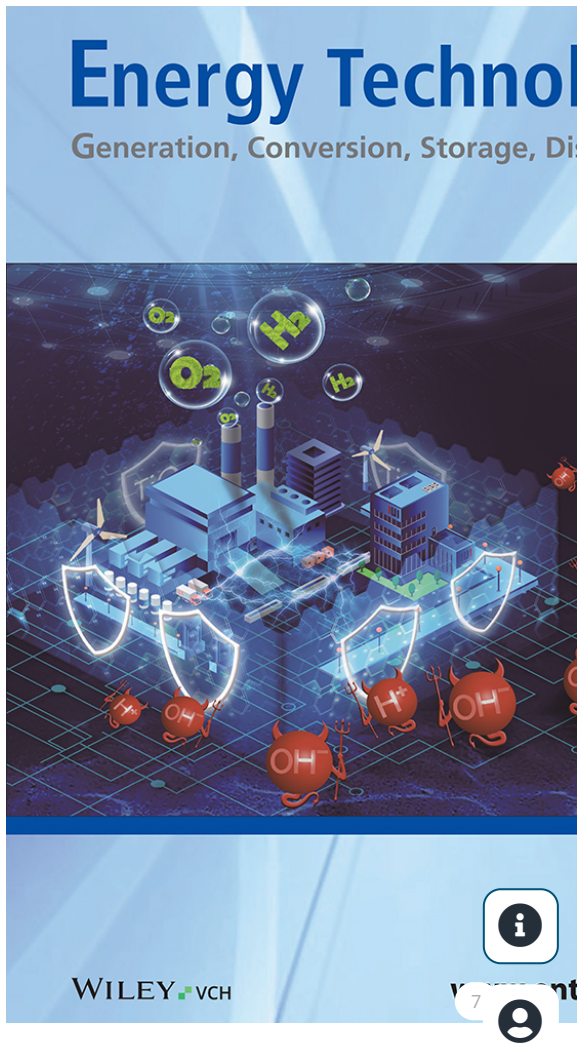

17 (2024): 18747–18756, https://doi.org/10.1021/acsomega.4c00709.

26. R. S. H. Yang, R. H. Garman, R. R. Maronpot, J. A. McKelvey, C. S. Weil, and M. D. Woodside, "Acute and Subchronic Toxicity of Ethylenediamine in Laboratory Animals." *Fundamental and Applied Toxicology* 3, no. 6 (1983): 512–520, https://doi.org/10.1016/S0272-0590(83)80097-9.

27. C.-K. Wang, C.-W. Hou, and Y.-X. Wei, *Degradation and Detoxicity of Ethylenediamine Wastewater by a Continuous Dosing Mode Sono-Fenton Process*;, *Sustainable Environment Research*, 23(2013):413–420

28. E. Andersson and B. Arbete Och Hälsa Järvholm, *National Institute for Working Life: Solna*. Sweden, 1994).

29. X. Chang, Y. Liu, Y. Ping, et al., "Multivalent Ligands Regulate Dimensional Engineering for Inverted Perovskite Solar Modules," *Science (New York, N.Y.)* 391, no. 6781 (2026): 153–159, https://doi.org/10.1126/science.aea0656.

30. H. Ali, I. Ahmed, K. Robertson, and A. E. Lanterna, "PDI-Functionalized Glass Beads: Efficient, Metal-Free Heterogeneous Photocatalysts Suitable for Flow Photochemistry," *Organic Process Research & Development*. (2024), https://doi.org/10.1021/acs.oprd.4c00256.

31. T. Adhikari, Z. Ghoshouni Rahami, J. M. Nunzi, and O. Synthesis Lebel, "Characterization and Photovoltaic Performance of Novel Glass-Forming Perylenediimide Derivatives," *Organic Electronics* 34 (2016): 146–156, https://doi.org/10.1016/j.orgel.2016.04.025.

32. D. S. Brar, R. Aponte, and J. Tunge, "Photoredox-Catalyzed Decarboxylative Elimination via Halogen Atom Transfer," *The Journal of Organic Chemistry* 90, no. 15 (2025): 5274–5280, https://doi.org/10.1021/acs.joc.5c00237.

33. R. Bhattacharjee, H. Jervis, M. E. McCormack, M. A. Petrukhina, and M. Kertesz, "Structure and Bonding in π-Stacked Perylenes: The Impact of Charge on Pancake Bonding," *Journal of the American Chemical Society* 146, no. 15 (2024): 10465–10477, https://doi.org/10.1021/jacs.3c14065.

34. S. Li, X. Wang, J. Fang, et al., "Interfacial Competing Interaction Eliminates Voids in the Buried Interface for Efficient and Stable Perovskite Solar Modules on Bare NiOX," *Chemical Engineering Journal* 490 (2024): 151919, https://doi.org/https://doi.org/10.1016/j.cej.2024.151919.

35. M. Zhai, Z. Guo, J. Yang, et al., "Interface Regulation with D-A-D Type Small Molecule for Efficient and Durable Perovskite Solar Cells," *Journal of Energy Chemistry* 107 (2025): 832–840, https://doi.org/https://doi.org/10.1016/j.jechem.2025.04.010.

36. A. Sharma, R. Singh, G. P. Kini, et al., "Side-Chain Engineering of Diketopyrrolopyrrole-Based Hole-Transport Materials to Realize High-Efficiency Perovskite Solar Cells," *ACS Applied Materials & Interfaces* 13, no. 6 (2021): 7405–7415, https://doi.org/10.1021/acsami.0c17583.

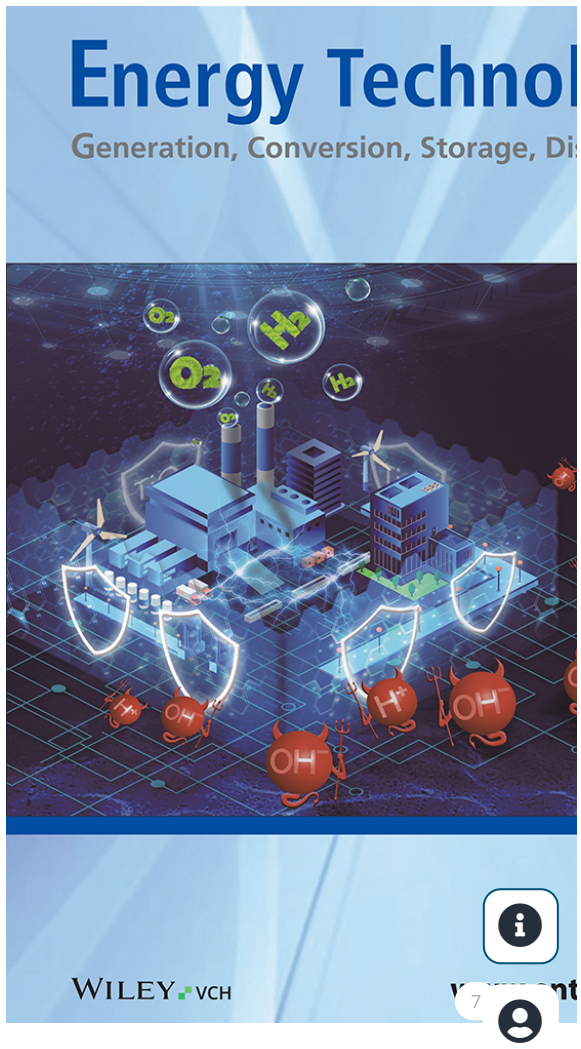

Perovskite Solar Cells," *Journal of Chemistry* 27, no. 4 (2018): 1175–1182, https://doi.org/https://doi.org/10.1016/j.jechem.2017.08.007.

38. G. P. Kini, M. Parashar, V. K. Shukla, and R. Singh, "Deciphering the Effect of Replacing Thiophene with Selenophene in Diketopyrrolopyrrole (DPP)-Based Low Cost Hole Transport Materials on the Performance of Perovskite Solar Cells," *Sustainable Energy & Fuels* 5, no. 23 (2021): 5994–6003, https://doi.org/10.1039/D1SE01211H.

39. T. Adhikari, J. M. Nunzi, and O. Lebel, "Solid-State Showdown: Comparing the Photovoltaic Performance of Amorphous and Crystalline Small-Molecule Diketopyrrolopyrrole Acceptors," *Organic Electronics* 48 (2017): 230–240, https://doi.org/10.1016/j.orgel.2017.06.008.

40. K. Amratisha, W. Tuchinda, P. Ruankham, et al., "Multilayer Triple Cation Perovskites for High Speed and Detectivity Self-Powered Photodetector via Scalable Spray Coating Process," *Scientific Reports* 12, no. 1 (2022), https://doi.org/10.1038/s41598-022-14774-x.

41. V. Cimrová, M. Guesmi, S. Eom, Y. Kang, and D. Výprachtický, "Formamidinium Lead Iodide Perovskite Thin Films Formed by Two-Step Sequential Method: Solvent–Morphology Relationship," *Materials* 16, no. 3 (2023), https://doi.org/10.3390/ma16031049.

42. F. Ma, J. Li, W. Li, N. Lin, L. Wang, and J. Qiao, "Stable α/δ Phase Junction of Formamidinium Lead Iodide Perovskites for Enhanced Near-Infrared Emission," *Chemical Science* 8, no. 1 (2017): 800–805, https://doi.org/10.1039/c6sc03542f.

43. T. Zhu and X. Gong, *Low-Dimensional Perovskite Materials and Their Optoelectronics*. InfoMat. Blackwell Publishing Ltd. October 1, 2021). 1039–1069, https://doi.org/10.1002/inf2.12211

44. O. E. Solis, M. Mínguez-Avellán, P. F. Betancur, et al., "Adjusting the Crystallization of Tin Perovskites through Thiophene Additives for Improved Photovoltaic Stability," *Acs Energy Letters*. (2024): 5288–5295, https://doi.org/10.1021/acsenergylett.4c01875.

45. J. Kim, A. J. Yun, B. Gil, Y. Lee, and B. Park, "Triamine-Based Aromatic Cation as a Novel Stabilizer for Efficient Perovskite Solar Cells," *Advanced Functional Materials* 29, no. 44 (2019), https://doi.org/10.1002/adfm.201905190.

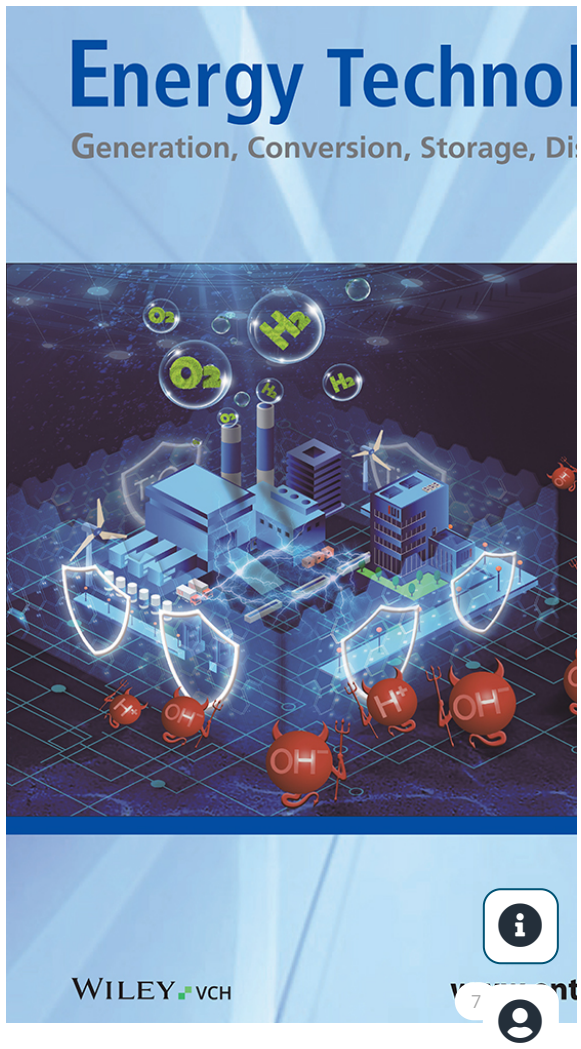

How to cite this article: Ersan Y. Muslih, Neng Hani Handayani, Masahiro Nakano, Makoto Karakawa, Mohammad Ismail Hossain, Md. Akhtaruzzaman, Jean-Michel Nunzi, Olivier Lebel, Tetsuya Taima, Md. Shahiduzzaman, *Energy Technology* 2026, 0 , e202502597. https://doi.org/10.1002/ente.202502597

----------End of Document----------

Research Article | Open Access

Molecular Glass Interface Engineering Enables Highly Efficient and Stable Inverted Perovskite Solar Cells

Ersan Y. Muslih, Neng Hani Handayani, Masahiro Nakano, Makoto Karakawa, Mohammad Ismail Hossain, Md. Akhtaruzzaman, Jean-Michel Nunzi, Olivier Lebel, Tetsuya Taima, Md. Shahiduzzaman

First published: 13 April 2026

https://doi.org/10.1002/ente.202502597

Abstract

Perovskite solar cells with inverted configuration (p–i–n) offer simple, low-temperature fabrication and high open-circuit voltage, but they are limited by poor thermal and moisture stability. Here, we introduce solution-processable amorphous molecular glass electron-acceptor interlayers, comprising two fused fluoranthene imide (FFI) derivatives and a diketopyrrolopyrrole (DPP) analog, which simultaneously enhance the efficiency and operational durability of $MAPbI_3$ p–i–n devices. These glassy films utilize strong π-π stacking, electron-withdrawing triazine and thiophene units, and inher

View PDF

to optimize energy-level alignment with PCBM, reduce ion migration, and prevent moisture ingress. The addition of FFI increases the champion power conversion efficiency (PCE) from 14.6% to 15.5% and raises the water contact angle from 77° to 108°. Under continuous maximum power point tracking at 85°C, FFI-modified cells retain over 90% of their initial PCE after 96 h, while control devices degrade within 48 h. X-ray diffraction and UV–Vis measurements confirm the sustained integrity of the α-phase and minimal formation of PbI_2. This interfacial engineering approach offers a scalable pathway to high-performance, durable perovskite photovoltaics.

1 Introduction

Perovskite solar cells (PSCs) have emerged as one of the most promising photovoltaic technologies due to their high-power conversion efficiency (PCE) exceeding 26% for n–i–p and p–i–n structure [1-6] yet with a low fabrication cost. However, their commercialization is hindered by stability issues and the need for efficient electron transport layers (ETLs) to

Back

interfacial mismatch, and photocatalytic activity are incompatible with perovskite films and it is not appropriate for hole-transport [7-11]. Thus, in p–i–n structure, ETLs, such as phenyl–C_{61}–butyric acid methyl ester (PCBM), are a common material due to low application temperature. In addition, PCBM molecules, whether blended into the bulk or added as a single layer as ETLs in devices, enhance electron transfer and can effectively reduce hysteresis [12-18]. However, the PCBM still has some shortcomings, such as it can still react with methylammonium iodide (MAI) or iodine ions, cannot repel H_2O molecules from outside, and even PCBM can penetrate into the perovskite grain boundaries, resulting in damage to the perovskite and a decrease in device performance [19-23]. Thus, interfacial modification with interlayer material helps protect the perovskite layer from ion migration and moisture-induced degradation, thereby improving long-term stability.

Interface modification has long been explored as a key strategy to improve both the efficiency and stability of PSCs. Among the reported approaches, ethylenediamine (EDA) has been used in Sn–Pb perovskites, where it successfully reduces trap states and enhances charge extraction [24]. Although ethylenediamine (EDA) has been reported to reduce interfacial trap states and facilitate charge extraction in perovskite-based devices, its practical applicability remains constrained by intrinsic material limitations, including high volatility, strong chemical reactivity, and well-documented corrosive and sensitizing properties, which raise concerns regarding handling safety and long-term interfacial stability [25-28]. By contrast, the molecular glass electron-acceptor compounds introduced in this work provide a distinct and advantageous alternative. Unlike EDA, these materials are structurally robust, nonvolatile, and capable of forming amorphous glassy interlayers that intimately coat the perovskite surface. Furthermore, they integrate defect passivation with additional functionalities, including hydrophobic protection, suppression of ion migration, and improved compatibility with PCBM. As a result, the molecular glass electron-acceptor compounds represent an evolutionary step in interfacial engineering, merging the defect passivation of earlier strategies, the multifunctionality of bifunctional ligands, and the robustness of glass-forming molecular systems. Collectively, these unique features establish them as a promising route toward achieving high-performance and durable PSCs. In the context of ligand-engineered PSCs, π–π interactions between aromatic moieties of multivalent ligands and the perovskite surface can enhance interfacial ordering and stability by promoting more uniform low-dimensional passivation layers, which in turn contribute to improved defect passivation and charge transport properties [29].

View PDF

In this study, we present molecular glass electron-acceptor derivatives as potential interlayer materials between perovskite and PCBM in a p–i–n structure, and thoroughly examine their influence on device performance. These molecular glass derivatives are especially appealing due to their strong π-bonding, extended delocalization, and inherent hydrophobic properties. Additionally, they showcase excellent electron mobility, high

distinct electronic and chemical interactions of the molecular glass interlayers prevent the degradation of methylammonium lead iodide ($MAPbI_3$) into lead iodide (PbI_2). Consequently, adding these materials not only boosts the efficiency of PSCs but also greatly enhances their operational stability.

2 Experimental Section

2.1 Materials

The fluorine-doped tin oxide (FTO) glass, with a thickness of 0.7 mm, resistivity of 9–10 Ω per square, and transmittance of 82–85%, was obtained from Nippon Sheet Glass Co., Ltd. (Tokyo, Japan). Acetone (C_3H_6O, 99.5% purity) and isopropanol (IPA, C_3H_8O, 99.5% purity) were sourced from Tokyo Chemical Industry Co., Ltd. (Tokyo, Japan). Lead iodide (PbI_2, 99.9% purity) was acquired from Tokyo Chemical Industry (Tokyo, Japan). *N*, *N*-dimethylformamide (DMF, 99.5% purity) were supplied by Wako Chemical (Tokyo, Japan). Dimethyl sulfoxide (DMSO, 99.5% purity), nickel nitrate pentahydrate ($Ni(NO_3)_2{\cdot}5H_2O$, 99.9% purity), methylammonium iodide (MAI, anhydrous, >99.9% purity), and ethanol (C_2H_6O, >99.9% purity) were obtained from Merck. Furthermore [6], -phenyl–C_{61}–butyric acid methyl ester (PCBM, 99.9%) and bathocuproine (BCP, 99.99%) were sourced from Sigma-Aldrich (Tokyo, Japan). Silver wire (Ag, 99.999% purity) was procured from Nilaco Corp. (Tokyo, Japan). Electron acceptors used were either previously published [31] or the complete synthetic details can be found in the Supporting Information.

2.2 Device Fabrication

The NiO_x thin film was made by dissolving 29.08 mg of $Ni(NO_3)_2{\cdot}5H_2O$ in 1 [illegible] 99.99% with constant stirring at 1000 rpm, then followed by filtering with PTFE 0.45 µ to filter some insoluble particles. The NiO_x thin film, serving as the hole transport layer, was deposited onto FTO-coated glass. The substrate was thoroughly cleaned using deionized water, acetone, and isopropyl alcohol, each undergoing 15 min of sonication. Afterward, it was dried with a nitrogen jet and subjected to plasma cleaning in an ozone atmosphere for 20 min. Subsequently, 100 µL of NiO_x precursor solution was dropped onto the substrate and evenly distributed using a spin-coater at 4000 rpm for 30 s, followed by annealing at 350°C for 3 h. The inverted PSCs were fabricated by depositing a precursor solution containing 1 M PbI_2 and 1 M MAI dissolved in 700 µL DMF and 300 µL DMSO, which had been stirred at 60°C for 12 h. This solution was spin coated onto a NiO_x thin film (acting as the hole transport layer) at 6000 rpm for 45 s, followed by annealing at 100°C for 15 min. Before deposition, the NiO_x layer underwent plasma cleaning in an ozone atmosphere for 10 min. Next, 20 mg/mL FFI or DPP compounds in chlorobenzene were deposited on perovskite using a spin coater at 2000 rpm for 30 s, and continued by drying at 105°C. Moreover, PCBM in chlorobenzene and 0.5 mg/mL BCP in ethanol were sequentially deposited via spin

10^{-4} Pa. The final device configuration was: glass/FTO/NiO_x/$MAPbI_3$/molecular glass electron-acceptor compounds/PCBM/BCP/Ag.

3 Results and Discussion

Various small-molecule electron-acceptor derivatives can improve the performance of perovskite-based solar cells. Small-molecule electron acceptors are promising because they have multiple conjugated and delocalized double bonds, making them suitable as ETLs in PSCs. The materials developed by our group are even more unique due to their glass-forming properties, which allow them to be deposited from solution as amorphous thin films. In this study, two new glass-forming fused fluoranthene imide (FFI) derivatives **1** and **2**, along with previously reported as diketopyrrolopyrrole (DPP) derivative **3** (3,3'-Bis(6-hexyl-1,3-dihydro-2H-indol-2-one)−2,2'-bithiophene-5,5'-dicarboxamide) [31], were studied. The structure of those materials is shown in Figure 1.

Back

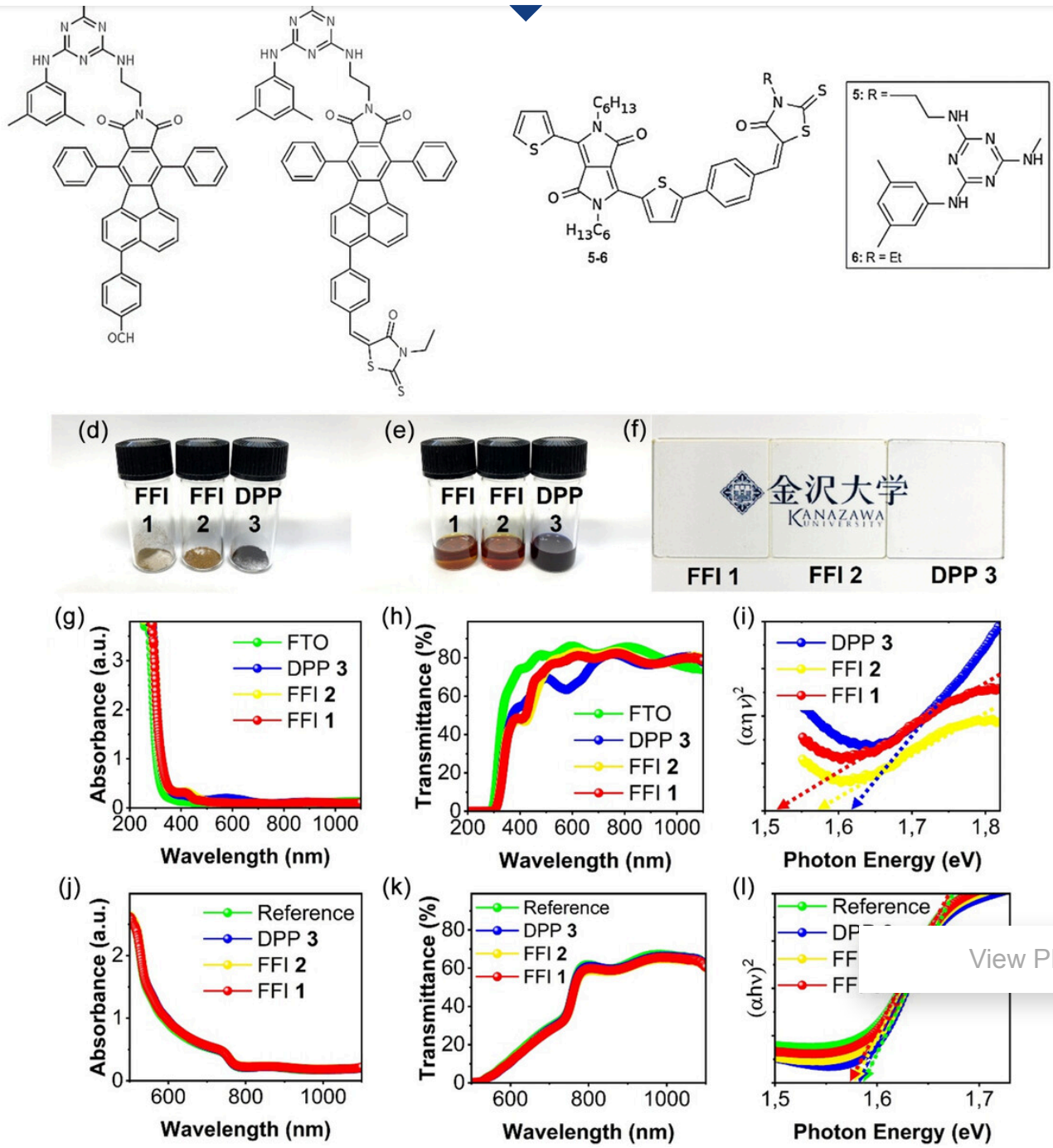

FIGURE 1

Open in figure viewer | PowerPoint

The structure of (a) FFI **1**, (b) FFI **2**, and (c) DPP **3**, and appearance of the compounds (d) before, (e) after dissolved in chlorobenzene, and its appearance (f) after deposited on glass. The optical properties of FFI **1**, FFI **2**, and DPP **3** for their (g) absorbance, (h) transmittance, and (i) Tauc plot, respectively. The optical properties of perovskite with FFI **1**, FFI **2**, and DPP **3** for its (j) absorbance, (k) transmittance, and (l) Tauc plot.

Back

naphthalene ring. Functionalizing the imide with the glass-inducing group enables a simple and divergent approach to screening different structures, even though it may not be optimal from a purely cost perspective. For this purpose, previously published amino glass **4** was converted to the corresponding maleimide **5** in 55% yield by condensation of the free $-NH_2$ group with maleic anhydride. This reaction was a half pathway to synthesis FFI **1** and FFI **2**. The reaction pathway is shown in Figure 2.

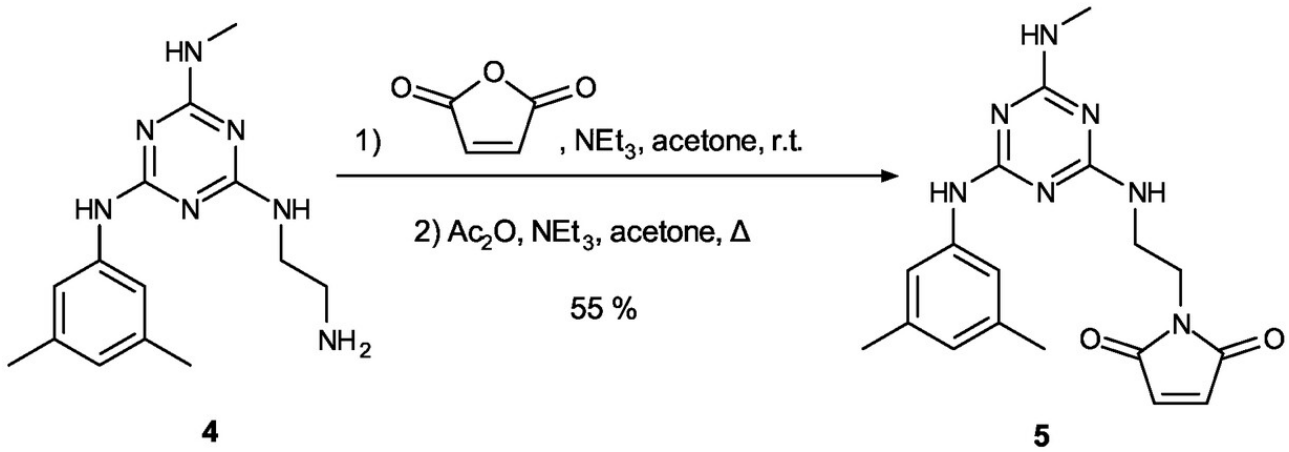

FIGURE 2

Open in figure viewer | PowerPoint

Synthesis reaction of maleimide compound from amino glass compound.

Moreover, maleimide glass **5** was then condensed via a cycloaddition reac cyclopentadienone **6** in refluxing nitrobenzene to afford mexylaminotriazine-substituted FFI glass **7** in 33% yield. Glass **7** is substituted with a bromo group on its naphthalene ring system, enabling further substitution with electron-withdrawing substituents to enhance its electron-acceptor character. A 4-formylphenyl group was introduced via Suzuki coupling to yield aldehyde 5, which was then condensed with *N*-ethylrhodanine to afford rhodanine-substituted FFI **6**, in 67 and 95% yields, respectively. Compounds **4** and **5** could be conveniently purified by simple filtration on a short silica pad, while FFI **6** could be purified by reprecipitation. The successful synthesis of the intermediate and final glass-forming compounds was confirmed by ^{1}H, ^{13}C, and HSQC NMR spectroscopy, displaying the expected chemical shifts and correlations for all major protons and carbons as shown in Figures S2–S13. The complete synthesis reaction of FFI **1** and FFI **2** is shown in Figure 3.

Back

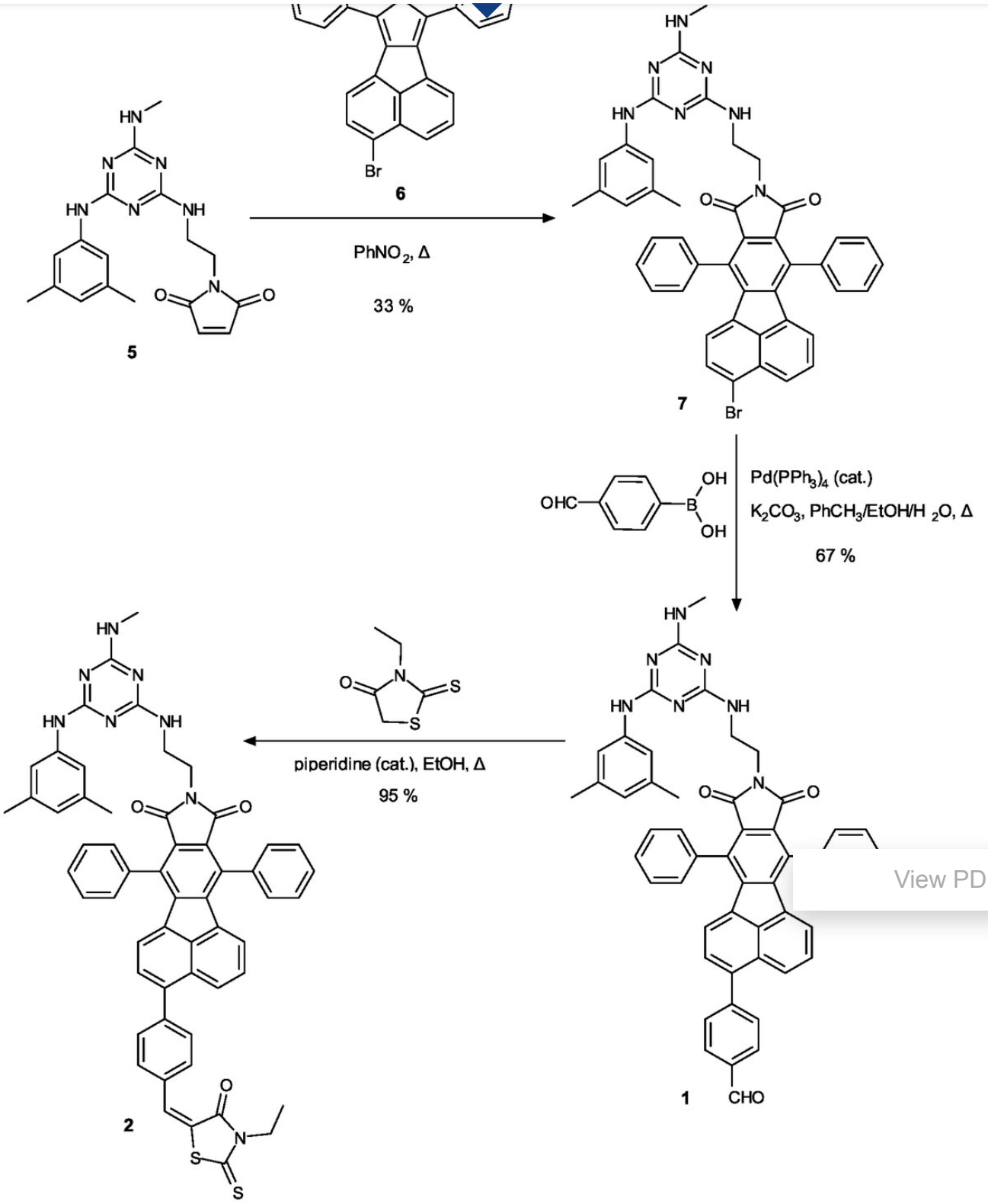

View PDF

FIGURE 3

Open in figure viewer | PowerPoint

Complete synthesis pathway of FFI **1** (shown as structure number 1) and FFI **2** (shown as structure number 2) from maleimide compound.

temperature (T_g) of 72°C, which is in the expected range for similar compounds. This glass-forming ability was successfully introduced in FFI derivatives **1–2** and **7**, which all showed T_g values ranging from 147 to 173°C, which are to be expected given the highly fused aromatic structures of the FFI moiety and the absence of long flexible chains. Again, no crystallization was observed for any of FFI glasses **1–2** and **7** under any conditions.

The UV–Vis spectrum data after depositing the molecular glass electron-acceptor compounds (FFI **1**, FFI **2**, and DPP **3**) on the perovskite layer reveal that the optical bandgap remains within the range from 1.57 to 1.58 eV, closely matching the reference perovskite layer. This stability in the bandgap suggests that the molecular glass electron-acceptor compounds do not significantly disrupt the perovskite's electronic structure. The absorption spectra of the molecular glass electron-acceptor compounds-modified perovskite layers closely follow the reference perovskite curve, indicating minimal alteration in optical properties and suggesting that these materials do not strongly absorb in the measured range. However, slight shifts or broadening at the absorption edge hint at potential interfacial interactions, such as charge transfer or dipole effects, which could influence carrier dynamics. The presence of these materials at the interface may modify charge transport and extraction without drastically affecting the intrinsic optical properties of the perovskite layer. These observations suggest that molecular glass electron-acceptor compounds could serve as functional interlayers in PSCs, optimizing charge transport while maintaining the fundamental absorption characteristics of the perovskite. The optical properties of perovskite modified by molecular glass electron-acceptor compounds are shown in Figure 1.

Furthermore, thermal stability test conducted over 96 h at 85 °C simultan… crucial insights into the effectiveness of molecular glass electron-acceptor compounds in enhancing the stability of perovskite materials. As shown in Figure 4, the perovskite films incorporated with molecular glass electron-acceptor compounds exhibit remarkable stability, maintaining their structural integrity and visual uniformity throughout the test period. This suggests that molecular glass electron-acceptor compounds may act as protective layers, mitigating thermal degradation by preventing ion migration, inhibiting moisture penetration, or reducing defect formation at the interface. Typically, perovskite materials are prone to degradation under prolonged thermal stress, leading to phase segregation, oxidation, or decomposition. However, the preserved appearance of the molecular glass electron-acceptor modified films indicates that these materials enhance the perovskite's resistance to thermal-induced degradation, potentially extending the operational lifetime of PSCs. Further analysis, such as UV–Vis spectra and X-ray diffraction (XRD), could confirm whether the structural and electronic properties remain intact, reinforcing the role of molecular glass electron-acceptor compounds in stabilizing perovskite materials under thermal stress. These findings highlight the potential of

Back

Figure 4 presents the UV–Vis spectra for the thermal stability of perovskite: (a) pristine perovskite as reference, perovskite with (b) FFI **1**, (c) FFI **2**, and (d) DPP **3**.

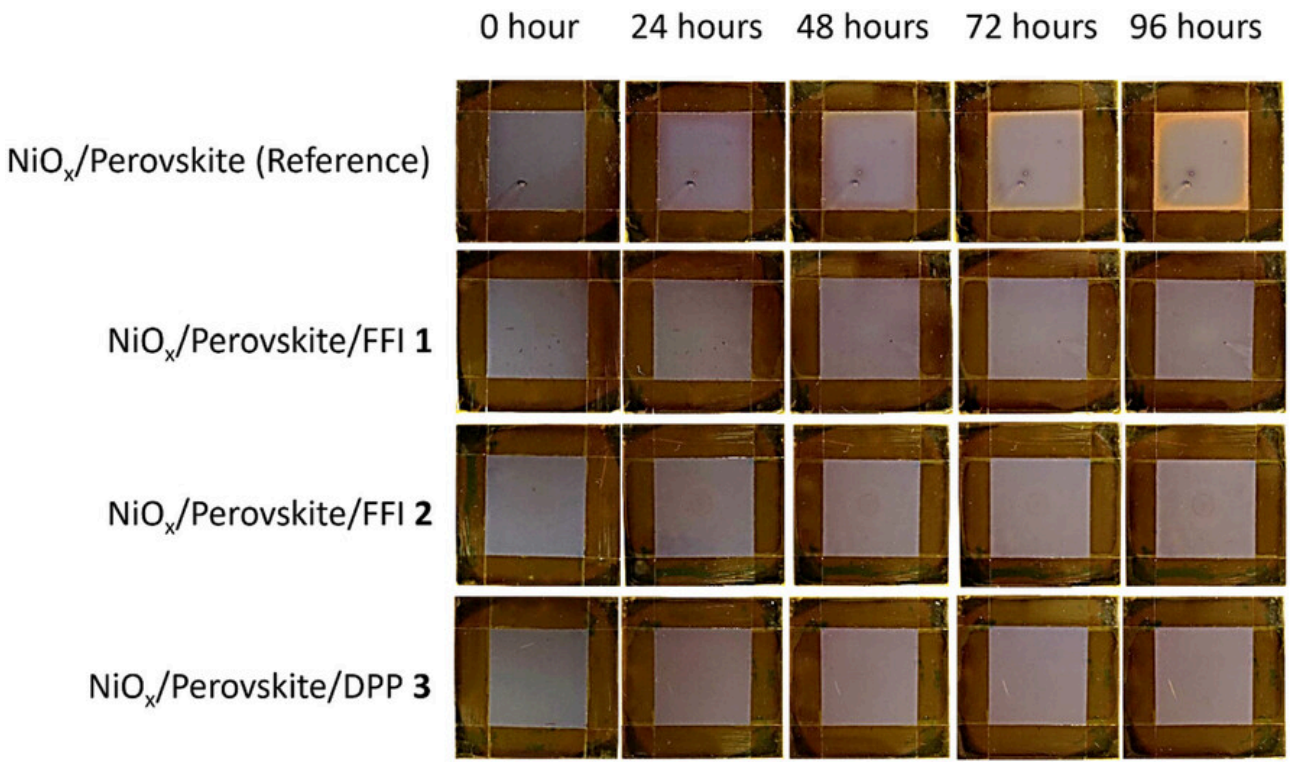

FIGURE 4

Open in figure viewer | PowerPoint

The appearance of perovskite with and without FFI **1**, **2**, and DPP **3** compounds on thermal sta

The complete set of UV–Vis spectra recorded during the 96-h thermal stability test is provided in the Supporting Information (Figure S14), which further confirms that the molecular glass-modified perovskite film retains its spectral profile and band edge positions, indicating suppressed thermal degradation compared to the pristine reference. The UV–Vis absorbance spectra shown in the image provide quantitative evidence supporting the thermal stability of perovskite materials incorporated with molecular glass electron-acceptor compounds over a 96-hour period at 85 ^{o}C. The absorbance curves at different time intervals (0 h, 24 h, 48 h, 72 h, and 96 h) show a gradual decrease in absorption intensity, a common characteristic of material degradation. However, the overall spectral shape and absorption edge remain relatively unchanged, indicating that the core optical properties of the perovskite layers are well preserved. Comparing these results with the thermal stability test images, it is evident that the molecular glass electron-acceptor compounds contribute to maintaining the structural and electronic integrity of the perovskite films. The minor reduction in absorbance suggests that some degradation occurs over time, likely due to

Back

molecular glass electron-acceptor compounds act as protective interlayers, reducing ion migration and preventing decomposition pathways that typically lead to perovskite degradation. Furthermore, the stability observed in the UV–Vis spectra implies that the bandgap energy of the perovskite remains nearly unchanged, ensuring that charge carrier generation and transport properties are not significantly compromised over the 96-hour test. This is crucial for the long-term performance of PSCs, as maintaining high absorption efficiency directly correlates with sustained photovoltaic performance. Figure S14 shows the impact of molecular glass electron-acceptor compounds on the perovskite layer under thermal stability test.

Moreover, Figure 5 illustrates the structural evolution and thermal stability of pristine and molecular glass-modified perovskite films during aging (0–96 hr), as revealed by XRD analysis. The XRD patterns compare pristine perovskite (a) with films incorporating molecular glass electron-acceptor additives FFI **1** (b), FFI **2** (c), and DPP **3** (d). The main diffraction peaks are marked with symbols, where α denotes the photoactive black α-phase perovskite, δ represents the undesired nonphotoactive δ-phase, and * indicates PbI_2, a typical degradation by-product. In the pristine film, the diffraction peak at $2\theta = 14.00°$, corresponding to the (100) plane, serves as the primary signature of the α-phase perovskite crystal structure, while the reflection at $2\theta = 20.11°$ is assigned to the (110) plane, representing a secondary but characteristic structural feature of halide perovskite [40-43]. Upon thermal exposure, the pristine sample exhibits pronounced structural degradation, as evidenced by the gradual attenuation of the α-phase reflections accompanied by the progressive emergence and intensification of the PbI_2 peak at 12.62°. Simultaneously, signatures of the δ-phase become more evident over time, indicating phase instability and partial transformation under thermal stress. This evolution reflects therm

iodide migration and defect-mediated decomposition, in which under-coordinated Pb^{2+} sites and halide vacancies act as nucleation centers for phase segregation toward PbI_2. The inset in Figure 5 highlights the evolution of the PbI_2 diffraction peak intensity over aging time, clearly demonstrating the accelerated degradation kinetics in the pristine film compared to the modified samples.

Back

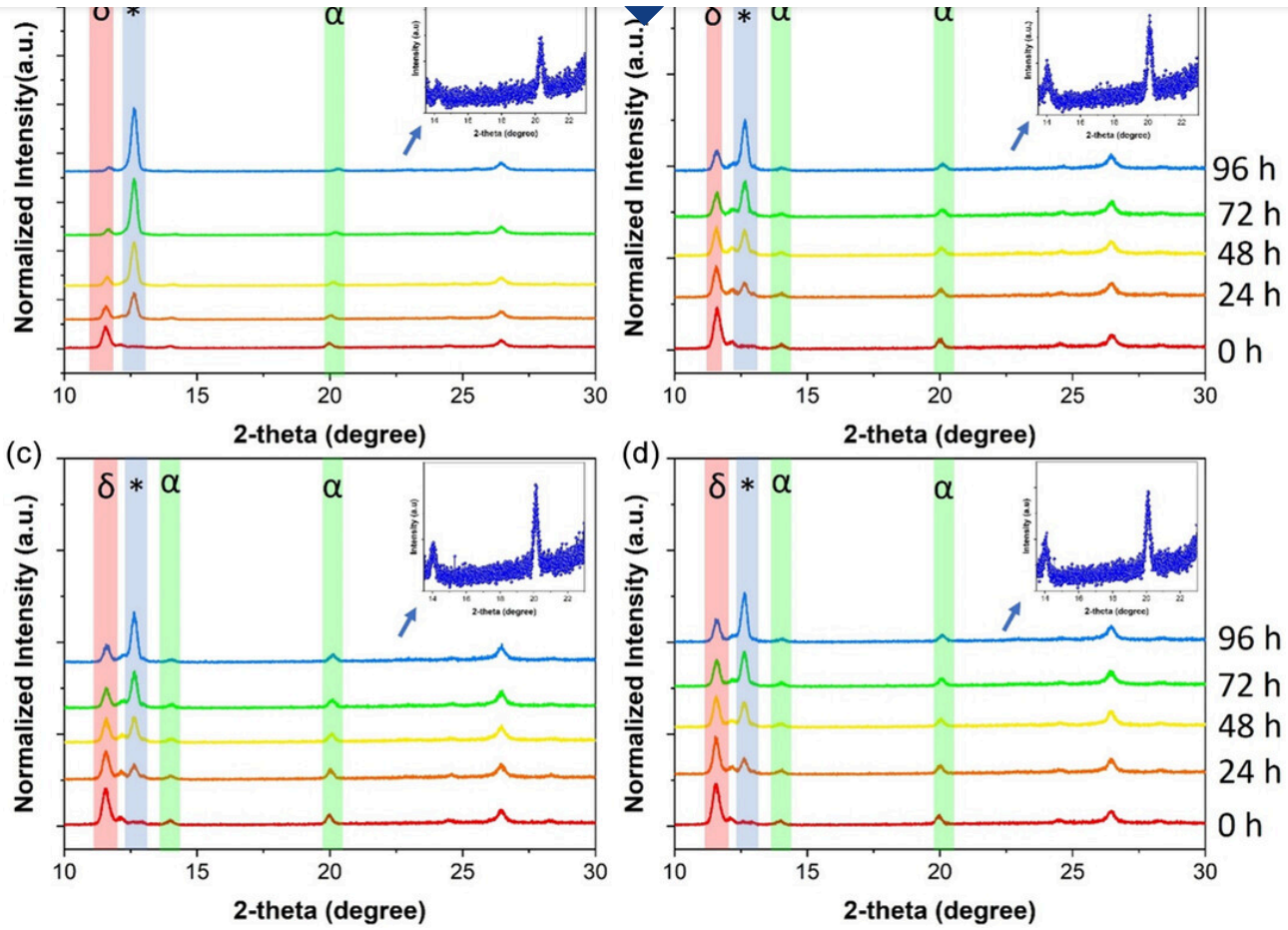

FIGURE 5

Open in figure viewer | PowerPoint

Evolution of the crystal structure and phase stability of perovskite films during thermal aging a
analyzed by X-ray diffraction (XRD). (a) Pristine perovskite (reference), (b) perovskite with FFI 1,
FFI 2, and (d) perovskite with DPP 3.

In contrast, the incorporation of molecular glass additives substantially mitigates these degradation pathways. The *α*-phase diffraction peaks remain comparatively stable in intensity over 96 hr, and the growth of the PbI_2 peak is markedly suppressed relative to the pristine film, demonstrating improved resistance to thermally induced phase segregation. The slower structural evolution observed in the modified films suggests that the molecular glass reduces defect density and stabilizes the perovskite lattice. Mechanistically, this enhancement can be attributed to several synergistic effects: coordination between molecular glass molecules and under-coordinated Pb^{2+} centers, which passivates structural defects; formation of an amorphous intergranular network that reinforces grain boundaries and limits lattice distortion; and suppression of halide ion migration, thereby inhibiting the autocatalytic decomposition process that typically accelerates degradation at elevated temperatures. Collectively, these effects kinetically and thermodynamically stabilize the

Back

The mechanism of perovskite decomposition has been extensively discussed by many researchers, with one of the main causes being the reaction between perovskite and water. Perovskite can also decompose into MAI and PbI_2. MAI can diffuse into the PCBM layer or evaporate as a gas, leaving behind yellow-colored PbI_2 as a degradation residue. Therefore, the structural degradation of perovskite can also be visually identified by changes in its color. If the perovskite layer begins to turn yellow, it indicates the formation of PbI_2, signaling the onset of decomposition. However, this phenomenon does not occur in perovskite layers that incorporate molecular glass electron-acceptor compounds. Molecular glass electron-acceptor compounds are well known for their extensive π-conjugated systems, which enable strong π–π interactions, resulting in enhanced electron delocalization and mobility. This feature is crucial for ETLs, as it enables efficient charge extraction from the perovskite layer to the electrode, minimizing charge recombination. The molecular glass electron-acceptor compounds have highly planar structures, promoting tight molecular packing and superior charge transport properties compared to conventional organic ETLs like PCBM.

Moreover, when molecular glass electron-acceptor compounds are introduced, a perovskite–molecular glass electron-acceptor compounds interface layer forms, exhibiting hydrophobic properties. This hydrophobicity arises from the extensive conjugated and delocalized bonds within the molecular glass electron-acceptor compounds, which effectively repel atmospheric water molecules and hydrophilic MAI molecules. This hydrophobicity can be seen from the contact angle of molecular glass electron-acceptor compounds on the perovskite surface in Figure 6, which increased from 77° in pristine perovskite to 107.0°, 108.4°, and 108.3° for FFI **1**, FFI **2**, and DPP **3**, respect

MAI does not diffuse into the PCBM layer or escape into the environment, leading to improved perovskite stability. The contact angles of water on molecular glass electron-acceptor compounds on perovskite are shown in Figure 6.

Back

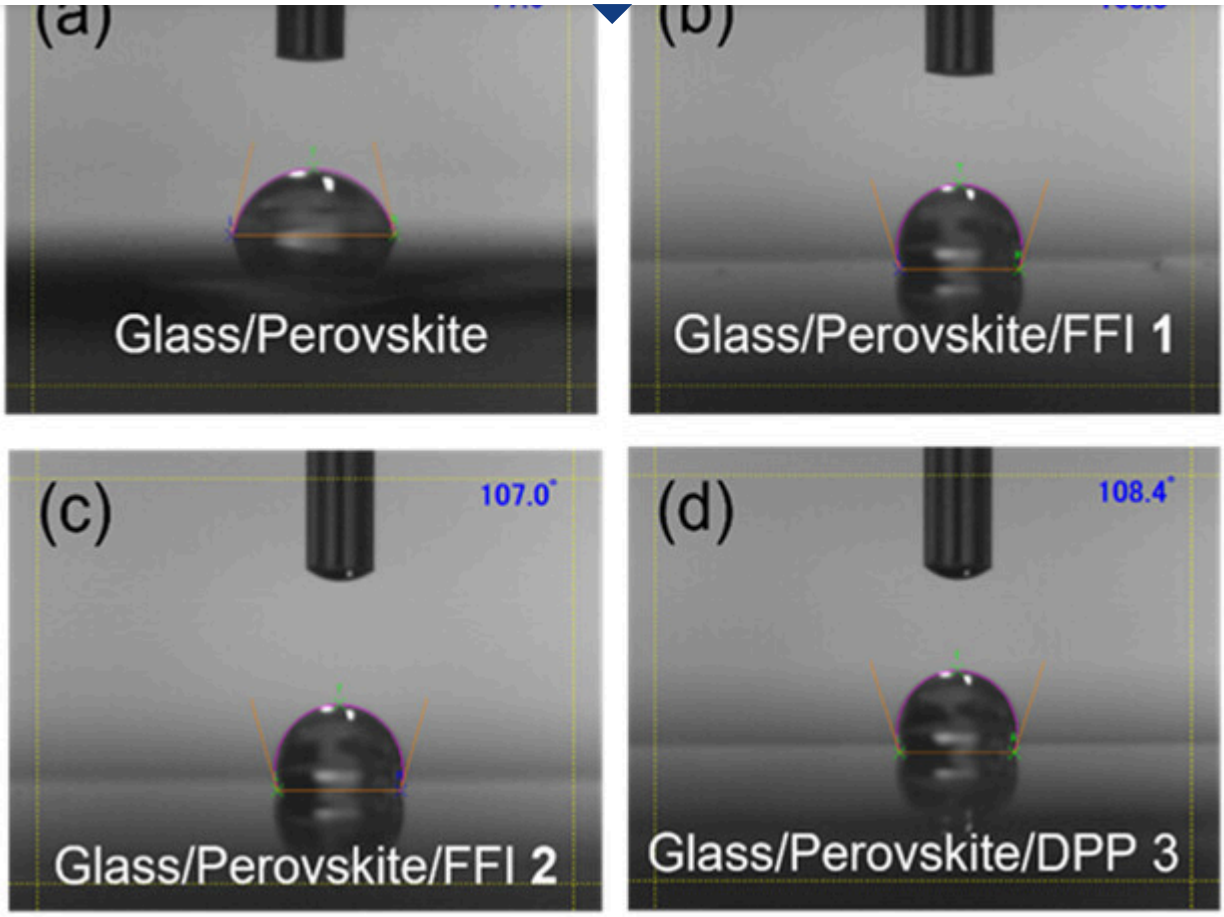

FIGURE 6

Open in figure viewer | PowerPoint

Contact angle test of perovskite with and without FFI **1**, FFI **2**, and DPP **3** compounds after 96 h

View PDF

Moreover, this hydrophobic perovskite–molecular glass electron-acceptor compounds interface enhances the compatibility between the perovskite and PCBM layers. This is because molecular glass electron-acceptor compounds share structural similarities with PCBM, including delocalized conjugated bonds and hydrophobicity, ensuring better interfacial contact. Additionally, molecular glass electron-acceptor compounds can still interact well with perovskite due to the triazine and thiophene functional groups, which can bind with the perovskite structure, further enhancing its stability. The decomposition and stability mechanisms are shown in Figure 7.

Back

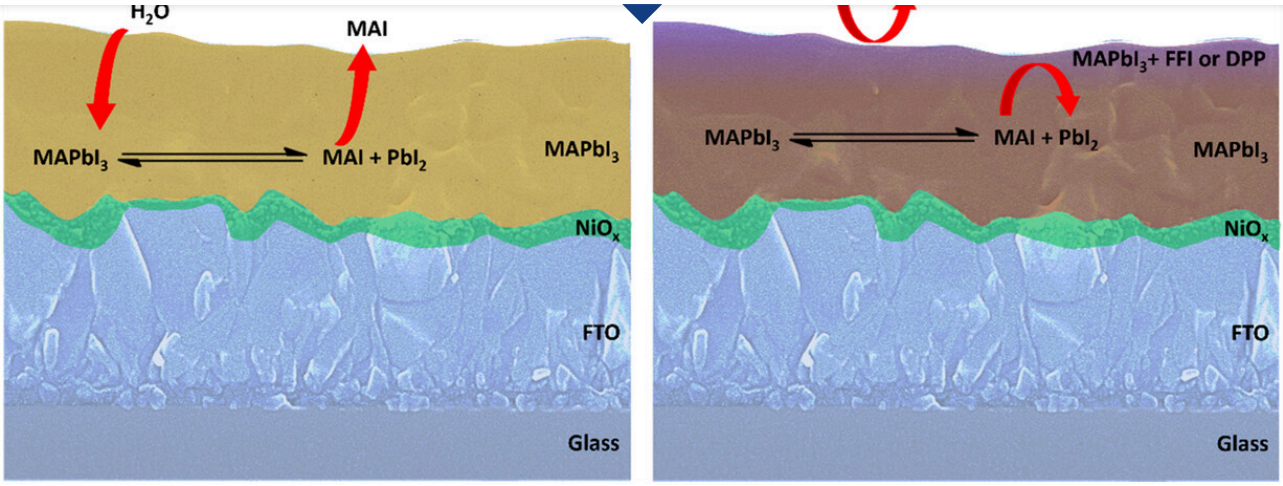

FIGURE 7

Open in figure viewer | PowerPoint

(a) The illustration of perovskite degradation on thermal stability test and (b) stability mechanism of perovskite due to added by molecular glass electron-acceptor compounds. The structure for thermal stability test was glass/FTO/NiO_x/$MAPbI_3$/molecular glass electron-acceptor compounds.

The hydrophobicity of molecular glass electron-acceptor compounds, resulting from conjugated and delocalized double bonds, enables them to repel external water molecules from the perovskite. This effectively suppresses perovskite degradation into MAI and PbI_2 while preventing MAI from reacting with PCBM and blocking PCBM diffusion into perovskite grain boundaries. Additionally, the molecular glass electron-acceptor compounds interlayer facilitates smooth electron migration from perovskite to PCBM, minimizin

These combined effects significantly enhance the long-term thermal stability of the perovskite film when molecular glass electron-acceptor compounds are used as ETLs.

Furthermore, scanning electron microscopy (SEM) images confirm that molecular glass electron-acceptor compounds effectively coat the perovskite surface and penetrate its grain boundaries, forming a protective hydrophobic layer. This encapsulation effect prevents moisture infiltration and thermal-induced degradation, thus improving the perovskite's resilience to environmental stressors. Consequently, the presence of molecular glass electron-acceptor compounds contributes to enhanced hydrophobicity and thermal stability, making this approach promising. Figure 8 shows the SEM image of pristine perovskite as a reference and perovskite added with molecular glass electron-acceptor compounds.

Back

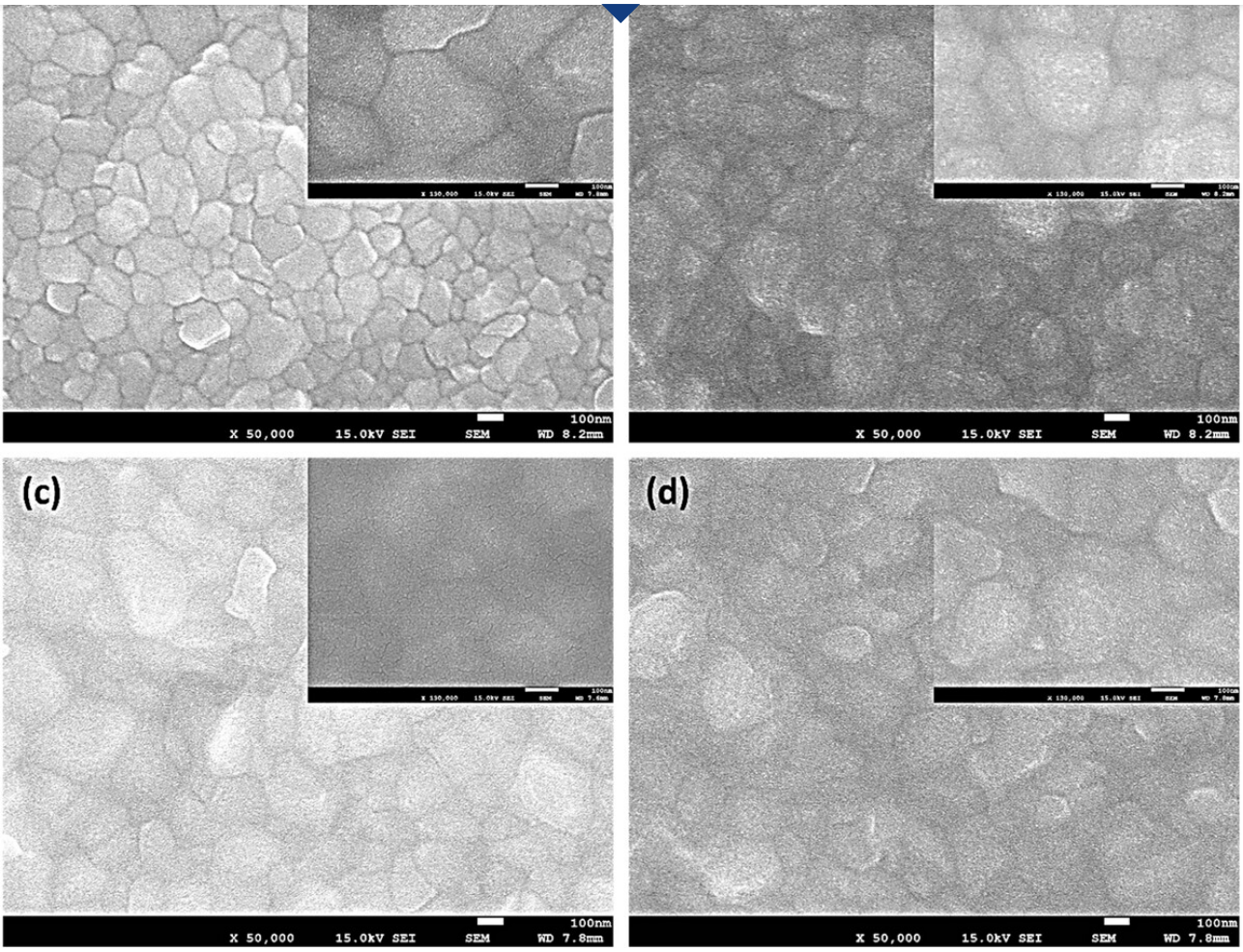

FIGURE 8

Open in figure viewer | PowerPoint

SEM image of (a) pristine perovskite as a reference, perovskite with (b) FFI **1**, (c) FFI **2**, and (d) D

electron microscopy.

Figure 9a presents the reverse scan *J–V* characteristics of PSCs fabricated without additives and with molecular glass electron-acceptor compounds. The plots clearly demonstrate variations in *Jsc* and *Voc* depending on the incorporated molecular glass. The reference device yields a *Jsc* of 17.86 mA/cm [2] and a *Voc* of 1.06 V, values typical of pristine PSCs. Upon the addition of molecular glass, the *J–V* behavior is distinctly modified. Among all samples, the device with FFI **1** achieves the highest *Jsc*, suggesting more efficient charge generation and extraction. This improvement can be attributed to enhanced film quality, higher crystallinity, and suppression of trap-assisted recombination. FFI **2** and DPP **3** also produce stable *J–V* curves with comparable *Voc* to the reference, although their *Jsc* values remain slightly lower than that of FFI **1**. In particular, the performance of DPP **3** is close to the reference, reflecting modest gains in current density but improved device stabilization.

Back

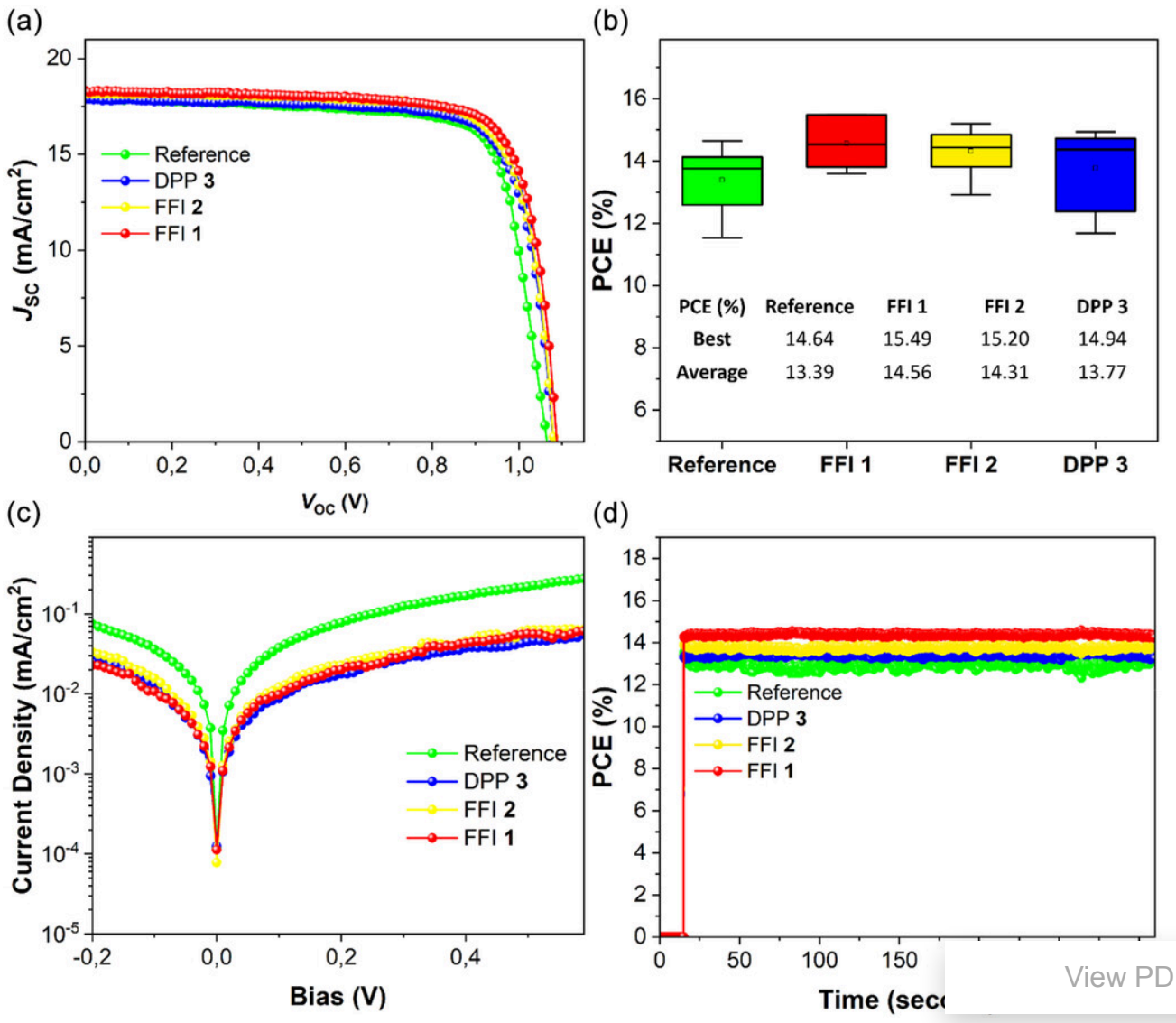

FIGURE 9

Open in figure viewer | PowerPoint

(a) The reverse scan *J–V* characteristics of PSCs fabricated without additives and with molecular glass additives FFI **1**, FFI **2**, and DPP **3**, (b) PCE comparison of pristine perovskite as reference, FFI **1**, FFI **2**, and DPP **3**, (c) comparison of dark *I–V* curve with and without molecular glass electron-acceptor compounds and (d) comparison MPPT curve perovskite with and without molecular glass electron-acceptor compounds. PCE = Power conversion efficiency.

The *J–V* data further reveal improvements across all key photovoltaic parameter (PCE, *Jsc*, *Voc*, and FF) when molecular glass-based interlayers are introduced. Notably, FFI **2** records the highest *Jsc* of 18.50 mA/cm [2], demonstrating superior charge collection. Meanwhile, *Voc* increases slightly to 1.08 V for both FFI **1** and FFI **2**, indicating better energy-level alignment between the perovskite absorber and ETL. The fill factor remains stable across

Back

scans further suggests the suppression of ion migration and improved interfacial charge transport. These effects are corroborated in Figure S15, which compares *J–V* curves at maximum PCE for devices with and without molecular glass. The molecular design of these additives plays a crucial role in enhancing performance. Triazine moieties provide strong electron-withdrawing properties, resulting in favorable energy-level alignment with the perovskite conduction band and facilitating efficient electron injection. Thiophene units, on the other hand, contribute molecular flexibility and improved charge transfer, which enhance overall transport characteristics [44, 45]. As a result, the modified devices achieve higher PCEs than the reference: FFI **1** reaches 15.49% (reverse scan), followed by FFI **2** at 15.20% and DPP **3** at 14.94%. These improvements demonstrate the ability of molecular glass electron-acceptor compounds to enhance charge extraction and mitigate recombination losses, as shown in Figure 9b. Further insights are obtained from the dark *I–V* characteristics. Molecular glass-based devices exhibit significantly reduced leakage currents compared to the reference, confirming better charge-blocking capability and suppression of recombination at the interfaces. The presence of triazine and thiophene groups within the interlayer enhances charge mobility and energy-level alignment, facilitating efficient electron transfer from the perovskite to PCBM. Lower dark current indicates effective suppression of ion migration and reduced charge accumulation, both of which contribute to improved interfacial stability and longer operational lifetimes, as shown in Figure 9c.

We further evaluated the impact of molecular glass interlayers on device stability using continuous maximum power point tracking (MPPT) measurements (Figure 9d). Compared with pristine devices, the molecular glass-modified perovskite-based devices exhibit higher and more stable power output under identical testing conditions, while the control devices show fast performance decay. The enhanced MPPT stability correlates wit

View PDF

thermal stability of the molecular glass-modified perovskite films (Figure 4), reduced leakage currents (Figure 9c), and suppressed thermally induced degradation. These consistent perovskite film modification and device-level trends confirm that the sustained MPPT performance arises from effective interfacial thermal stabilization. Overall, these results demonstrate that molecular glass electron-acceptor interlayers not only enhance device efficiency but also provide robust long-term operational stability with continuous MPPT serving as direct validation of the improved interfacial thermal robustness.

Moreover, the data clearly indicate the significant enhancement in device performance when molecular glass electron-acceptor compounds are introduced as an interfacial layer between perovskite and PCBM. The reference device, which employs only PCBM as the ETL, exhibits a moderate PCE, with relatively lower *Jsc* and *Voc*, likely due to suboptimal charge extraction and increased recombination at the interface. In contrast, PSCs modified with molecular glass electron-acceptor compounds show a substantial improvement in all key photovoltaic parameters. This improvement is attributed to the strong π–π stacking

energy level alignment and suppress interfacial defects. Among the FFI **1**, FFI **2**, and DPP **3**-based interlayers, FFI **2** demonstrates the highest PCE, indicating its superior ability to improve charge extraction and stability. The higher *Jsc* observed in FFI **2**-modified devices suggests more efficient electron collection, while the increase in *Voc* implies reduced nonradiative recombination losses. Moreover, the FF is significantly improved, signifying reduced series resistance and enhanced charge transfer dynamics. The DPP **3** and FFI **1** interlayers also exhibit improved performance compared to the reference, though slightly lower than FFI **2**, reinforcing the beneficial effects of FFI **1**, FFI **2**, and DPP **3** compounds. Table 1 provides a detailed comparison of the photovoltaic parameters such as PCE, *Jsc*, *Voc*, and FF for the reference device and PSCs integrated with various molecular glass compound interlayers.

TABLE 1. Comparison of *J–V* curve with and without molecular glass electron-acceptor compounds at best PCE.

Device	Scan direction	*Jsc* (mA/cm^2)	*Voc* (V)	FF	PCE (%)
Reference	Forward	17.54	1.06	0.75	14.01
	Reverse	17.95	1.06	0.77	14.64
FFI 1	Forward	18.44	1.08	0.76	15.17
	Reverse	18.32	1.08	0.78	15.49
FFI 2	Forward	18.50	1.07		
	Reverse	18.20	1.08		
DPP 3	Forward	18.05	1.07	0.76	14.61
	Reverse	17.87	1.07	0.78	14.94

4 Conclusions

This work demonstrates that glass-forming molecular electron-acceptor compounds are highly effective interfacial layers for inverted $MAPbI_3$-based PSCs. Molecular glass-modified perovskite films exhibit excellent thermal stability at 85°C for 96 hr, as confirmed by XRD, SEM, and UV–Vis analysis. Mechanistic insights reveal that strong π–π stacking, electron-withdrawing triazine/thiophene units, and amorphous glass-like morphology collectively enhance interfacial robustness. The increase in water contact angle from 77° to over 108° further indicates the formation of durable hydrophobic barriers that suppress MAI diffusion

Consequently, MPPT measurements demonstrate sustained and stable power output, confirming that the improved operational stability arises from the robust thermal and interfacial stabilization imparted by the molecular glass interlayers.

Supporting Information

Additional supporting information can be found online in the Supporting Information section. **Supporting Fig. S1:** HOMO and LUMO orbitals of FFI glasses **1** and **2** as calculated by DFT (B3LYP/6,31G(d,p)). The mexylaminotriazine group was omitted from the calculations since it contributes minimally to the electronics of the FFI chromophore. (a) HOMO orbital of glass **1**, (b) LUMO orbital of glass **1**, (c) HOMO orbital of glass **2**, (d) LUMO orbital of glass **2**. **Supporting Fig. S2:** ^{1}H NMR spectrum of compound 5 in DMSO-d_6 at 363K, 400 MHz. **Supporting Fig. S3:** ^{13}C NMR spectrum of compound **5** in DMSO-d_6, 75 MHz. **Supporting Fig. S4:** HSQC NMR spectrum of compound **5** in DMSO-d_6, 400 MHz. **Supporting Fig. S5:** ^{1}H NMR spectrum of compound **7** in DMSO-d_6 at 363K, 400 MHz. **Supporting Fig. S6:** ^{13}C NMR spectrum of compound **7** in DMSO-d_6, 75 MHz. **Supporting Fig. S7:** HSQC NMR spectrum of compound **7** in DMSO-d_6, 400 MHz. **Supporting Fig. S8:** ^{1}H NMR spectrum of compound **1** in DMSO-d_6 at 363K, 400 MHz. **Supporting Fig. S9:** ^{13}C NMR spectrum of compound **1** in DMSO-d_6, 75 MHz. **Supporting Fig. S10:** HSQC NMR spectrum of compound **1** in DMSO-d_6, 400 MHz. **Supporting Fig. S11:** ^{1}H NMR spectrum of compound **2** in DMSO-d_6 at 363K, 400 MHz. **Supporting Fig. S12:** ^{13}C NMR spectrum of compound **2** in DMSO-d_6, 75 MHz. **Supporting Fig. S13:** HSQC NMR spectrum of compound **2** in DMSO-d_6, 400 MHz. **Supporting Fig. S14:** UV-Vis spectra as thermal stability of perovskite after 96 hours: (a) Pristine perovskite as a reference, perovskite with (b) FFI **1**, (c) FFI **2**, and (d) DPP **3**. **Supporting Fig. S15:** Comparison of *J–V* curve perovskite with and without compounds at best PCE: (a) Pristine perovskite as a reference, perovskite with (b) FFI **1**, (c) FFI **2**, and (d) DPP **3**.

Acknowledgments

This study was partially supported by a Grant-in-Aid for Scientific Research (grant number 24K17769). Research at Queens was also supported by the the Natural Sciences and Engineering Research Council of Canada (RGPIN-2020−07016). The authors also extend their appreciation to the research support by the Deanship of Graduate Studies and Scientific Research at the Islamic University of Madinah, Saudi Arabia.

Funding

This study was partially supported by a Grant-in-Aid for Scientific Research (24K17769). Research at Queens was also supported by the the Natural Sciences and Engineering

Back

Research at the Islamic University of Madinah, Saudi Arabia.

Conflicts of Interest

The authors declare no conflicts of interest.

Data Availability Statement

A Data Availability Statement has now been included in the revised manuscript. The data supporting the findings of this study are available within the article and its supporting information. Additional data is available from the corresponding author upon reasonable request.

Supporting Information

Filename	Description
ente70451-sup-0001-SuppData-S1.pdf 1.3 MB	Supplementary Material

Please note: The publisher is not responsible for the content or functionality of any supporting information supplied by the authors. Any queries (other than missing content) should be directed to the corresponding author for the article.

View PDF

References

1 J. Zhou, L. Tan, Y. Liu, et al., "Highly Efficient and Stable Perovskite Solar Cells via a Multifunctional Hole Transporting Material," *Efficient and Stable Perovskite Solar Cells via a Multifunctional Hole Transporting Material. Joule* **8**, no. 6 (2024): 1691–1706, https://doi.org/10.1016/J.JOULE.2024.02.019.

CAS | Google Scholar

2 H. Chen, C. Liu, J. Xu, et al., "Improved Charge Extraction in Inverted Perovskite Solar Cells with Dual-Site-Binding Ligands," *Science (New York, N.Y.)* **384**, no. 6692 (1979. 2024): 189–193, https://doi.org/10.1126/SCIENCE.ADM9474/SUPPL_FILE/SCIENCE.ADM9474_SM.PDF.

Google Scholar

Back

CAS | PubMed | Web of Science® | Google Scholar

4 R. Azmi, E. Ugur, A. Seitkhan, et al., "Damp Heat–Stable Perovskite Solar Cells with Tailored-Dimensionality 2D/3D Heterojunctions," *Science (New York, N.Y.)* **376**, no. 6588 (2022): 73–77, https://doi.org/10.1126/science.abm5784.

CAS | PubMed | Web of Science® | Google Scholar

5 X. Liu, B. Zheng, L. Shi, et al., "Perovskite Solar Cells Based on Spiro-OMeTAD Stabilized with an Alkylthiol Additive," *Nature Photonics* **17**, no. 1 (2023): 96–105, https://doi.org/10.1038/s41566-022-01111-x.

CAS | Web of Science® | Google Scholar

6 S. Gong, G. Qu, Y. Qiao, et al., "A Hot Carrier Perovskite Solar Cell with Efficiency Exceeding 27% Enabled by Ultrafast Hot Hole Transfer with Phthalocyanine Derivatives," *Energy & Environmental Science* **17**, no. 14 (2024): 5080–5090, https://doi.org/10.1039/D4EE01839G.

CAS | Web of Science® | Google Scholar

7 V. J. Garcia, C. M. Pelicano, and H. Yanagi, "Low Temperature-Processed ZnO Nanorods-TiO2 Nanoparticles Composite as Electron Transporting Layer for Perovskite Solar Cell**s** **662** (2018): 70–75, https://doi.org/10.1016/J.TSF.2018.07.039.

CAS | Web of Science® | Google Scholar

8 A. A. Qureshi, H. M. A. Javed, S. Javed, et al., "Incorporation of Zr-Doped TiO_2 Nanoparticles in Electron Transport Layer for Efficient Planar Perovskite Solar Cells," *Surfaces and Interfaces* **25** (2021): 101299, https://doi.org/10.1016/J.SURFIN.2021.101299.

CAS | Web of Science® | Google Scholar

9 L. K. Ono, E. J. Juarez-Perez, and Y. Qi, "Progress on Perovskite Materials and Solar Cells with Mixed Cations and Halide Anions," *ACS Applied Materials and Interfaces. American Chemical Society September* **9** (2017): 30197–30246, https://doi.org/10.1021/acsami.7b06001.

CAS | PubMed | Web of Science® | Google Scholar

Back

CAS | Web of Science® | Google Scholar

11 M. Gantumur, M. Shahiduzzaman, M. I. Hossain, et al., "Revolutionizing Light Capture: A Comprehensive Review of Back-Contact Perovskite Solar Cell Architectures," *T. Revolutionizing Light Capture: A Comprehensive Review of Back-Contact Perovskite Solar Cell Architectures. Materials Today. Elsevier B.V.* (2025), https://doi.org/10.1016/j.mattod.2025.08.017.

Google Scholar

12 Y. Zhong, M. Hufnagel, M. Thelakkat, C. Li, and S. Huettner, "Role of PCBM in the Suppression of Hysteresis in Perovskite Solar Cells," *Advanced Functional Materials* **30** (2020): 23, https://doi.org/10.1002/adfm.201908920.

Web of Science® | Google Scholar

13 F. Zhang, W. Shi, J. Luo, et al., "Isomer-Pure Bis-PCBM-Assisted Crystal Engineering of Perovskite Solar Cells Showing Excellent Efficiency and Stability," *Advanced Materials* **29**, no. 17 (2017): 1606806, https://doi.org/10.1002/ADMA.201606806.

Web of Science® | Google Scholar

14 Y. Shao, Z. Xiao, C. Bi, Y. Yuan, and J. Huang, "Origin and Elimination of Photoc
by Fullerene Passivation in CH3NH3PbI3 Planar Heterojunction Solar Cells," *Natur*
5 (2014), https://doi.org/10.1038/ncomms6784.

View PDF

Web of Science® | Google Scholar

15 E. Bi, H. Chen, F. Xie, et al., "Diffusion Engineering of Ions and Charge Carriers for Stable Efficient Perovskite Solar Cells," *Nature Communications* **8** (2017), https://doi.org/10.1038/ncomms15330.

Web of Science® | Google Scholar

16 K. Wojciechowski, S. D. Stranks, A. Abate, et al., "Modification for Highly Efficient Organic-Inorganic Perovskite Solar Cells," *ACS Nano* **8**, no. 12 (2014): 12701–12709, https://doi.org/10.1021/NN505723H/SUPPL_FILE/NN505723H_SI_001.PDF.

CAS | PubMed | Web of Science® | Google Scholar

Back

Express **15**, no. 1 (2022): 015504, https://doi.org/10.35848/1882-0786/ac435d.

CAS | Google Scholar

18 M. J. M. Marques, W. Lin, T. Taima, S. Umezu, and M. Shahiduzzaman, *Unleashing the Potential of Industry Viable Roll-to-Roll Compatible Technologies for Perovskite Solar Cells: Challenges and Prospects. Materials Today* (Elsevier B.V, September 1, 2024), 112–141, https://doi.org/10.1016/j.mattod.2024.06.013

Google Scholar

19 L. Shen, P. Song, K. Jiang, et al., "Ultrathin Polymer Membrane for Improved Hole Extraction and Ion Blocking in Perovskite Solar Cells," *Nature Communications* **15**, no. 1 (2024), https://doi.org/10.1038/s41467-024-55329-0.

Web of Science® | Google Scholar

20 C. Gong, H. Li, H. Wang, et al., "Coordination-Induced n-Doping of PCBM for Stable and Efficient Inverted Perovskite Solar Cells," *Nature Communications* **15**, no. 1 (2024), https://doi.org/10.1038/s41467-024-49395-7.

Web of Science® | Google Scholar

21 Z. Shen, Q. Han, X. Luo, et al., "Efficient and Stable Perovskite Solar Cells with Depletion Region," *Nature Photonics* **18**, no. 5 (2024): 450–457, https://doi.org/10.1038/s41566-024-01383-5.

CAS | Web of Science® | Google Scholar

22 S. You, F. T. Eickemeyer, J. Gao, et al., "Hole-Shuttle Molecule for Improved Interfacial Energy Level Alignment and Defect Passivation in Perovskite Solar Cells," *Nature Energy* **8**, no. 5 (2023): 515–525, https://doi.org/10.1038/s41560-023-01249-0.

CAS | Web of Science® | Google Scholar

23 Md Shahiduzzaman, E. Y. Muslih, A. K. M. Hasan, et al., "The Benefits of Ionic Liquids for the Fabrication of Efficient and Stable Perovskite Photovoltaics," *Chemical Engineering Journal* **411** (2021): 128461, https://doi.org/https://doi.org/10.1016/j.cej.2021.128461.

Back

24 G. Kapil, T. Bessho, T. Maekawa, et al., "Tin-Lead Perovskite Fabricated via Ethylenediamine Interlayer Guides to the Solar Cell Efficiency of 21.74%," *Advanced Energy Materials* **11**, no. 25 (2021): 2101069, https://doi.org/https://doi.org/10.1002/aenm.202101069.

CAS | Web of Science® | Google Scholar

25 Y. Wu and H. Green An, "Catalytic Synthesis of Ethylenediamine from Ethylene Glycol and Monoethanolamine," *A Review. ACS Omega* **9**, no. 17 (2024): 18747–18756, https://doi.org/10.1021/acsomega.4c00709.

CAS | PubMed | Web of Science® | Google Scholar

26 R. S. H. Yang, R. H. Garman, R. R. Maronpot, J. A. McKelvey, C. S. Weil, and M. D. Woodside, "Acute and Subchronic Toxicity of Ethylenediamine in Laboratory Animals." *Fundamental and Applied Toxicology* **3**, no. 6 (1983): 512–520, https://doi.org/10.1016/S0272-0590(83)80097-9.

CAS | PubMed | Web of Science® | Google Scholar

27 C.-K. Wang, C.-W. Hou, and Y.-X. Wei, *Degradation and Detoxicity of Ethylenediamine Wastewater by a Continuous Dosing Mode Sono-Fenton Process*, *Sustainable Environment Research*, **23**(2013): 413–420

CAS | Google Scholar

28 E. Andersson and B. Arbete Och Hälsa Järvholm, *National Institute for Working Life. Solna*, (1994).

Google Scholar

29 X. Chang, Y. Liu, Y. Ping, et al., "Multivalent Ligands Regulate Dimensional Engineering for Inverted Perovskite Solar Modules," *Science (New York, N.Y.)* **391**, no. 6781 (2026): 153–159, https://doi.org/10.1126/science.aea0656.

CAS | PubMed | Web of Science® | Google Scholar

30 H. Ali, I. Ahmed, K. Robertson, and A. E. Lanterna, "PDI-Functionalized Glass Beads: Efficient, Metal-Free Heterogeneous Photocatalysts Suitable for Flow Photochemistry," *Organic Process Research & Development*, (2024): https://doi.org/10.1021/acs.oprd.4c00256.

PubMed | Web of Science® | Google Scholar

Back

34 (2016): 146–156, https://doi.org/10.1016/j.orgel.2016.04.025.

CAS | Web of Science® | Google Scholar

32 D. S. Brar, R. Aponte, and J. Tunge, "Photoredox-Catalyzed Decarboxylative Elimination via Halogen Atom Transfer," *The Journal of Organic Chemistry* **90**, no. 15 (2025): 5274–5280, https://doi.org/10.1021/acs.joc.5c00237.

CAS | Web of Science® | Google Scholar

33 R. Bhattacharjee, H. Jervis, M. E. McCormack, M. A. Petrukhina, and M. Kertesz, "Structure and Bonding in π-Stacked Perylenes: The Impact of Charge on Pancake Bonding," *Journal of the American Chemical Society* **146**, no. 15 (2024): 10465–10477, https://doi.org/10.1021/jacs.3c14065.

CAS | PubMed | Google Scholar

34 S. Li, X. Wang, J. Fang, et al., "Interfacial Competing Interaction Eliminates Voids in the Buried Interface for Efficient and Stable Perovskite Solar Modules on Bare NiOX," *Chemical Engineering Journal* **490** (2024): 151919, https://doi.org/https://doi.org/10.1016/j.cej.2024.151919.

CAS | Web of Science® | Google Scholar

35 M. Zhai, Z. Guo, J. Yang, et al., "Interface Regulation with D-A-D Type Small Mo and Durable Perovskite Solar Cells," *Journal of Energy Chemistry* **107** (2025): 832–8 https://doi.org/10.1016/j.jechem.2025.04.010.

CAS | Web of Science® | Google Scholar

36 A. Sharma, R. Singh, G. P. Kini, et al., "Side-Chain Engineering of Diketopyrrolopyrrole-Based Hole-Transport Materials to Realize High-Efficiency Perovskite Solar Cells," *ACS Applied Materials & Interfaces* **13**, no. 6 (2021): 7405–7415, https://doi.org/10.1021/acsami.0c17583.

CAS | PubMed | Web of Science® | Google Scholar

37 H. Cheng, X. Zhao, Y. Shen, et al., "Diketopyrrolopyrrole Based D-π-A-π-D Type Small Organic Molecules as Hole Transporting Materials for Perovskite Solar Cells," *Journal of Energy Chemistry* **27**, no. 4 (2018): 1175–1182, https://doi.org/https://doi.org/10.1016/j.jechem.2017.08.007.

Back

38 G. P. Kini, M. Parashar, V. K. Shukla, and R. Singh, "Deciphering the Effect of Replacing Thiophene with Selenophene in Diketopyrrolopyrrole (DPP)-Based Low Cost Hole Transport Materials on the Performance of Perovskite Solar Cells," *Sustainable Energy & Fuels* **5**, no. 23 (2021): 5994–6003, https://doi.org/10.1039/D1SE01211H.

CAS | Web of Science® | Google Scholar

39 T. Adhikari, J. M. Nunzi, and O. Lebel, "Solid-State Showdown: Comparing the Photovoltaic Performance of Amorphous and Crystalline Small-Molecule Diketopyrrolopyrrole Acceptors," *Organic Electronics* **48** (2017): 230–240, https://doi.org/10.1016/j.orgel.2017.06.008.

CAS | Web of Science® | Google Scholar

40 K. Amratisha, W. Tuchinda, P. Ruankham, et al., "Multilayer Triple Cation Perovskites for High Speed and Detectivity Self-Powered Photodetector via Scalable Spray Coating Process," *Scientific Reports* **12**, no. 1 (2022), https://doi.org/10.1038/s41598-022-14774-x.

PubMed | Web of Science® | Google Scholar

41 V. Cimrová, M. Guesmi, S. Eom, Y. Kang, and D. Výprachtický, "Formamidinium Lead Iodide Perovskite Thin Films Formed by Two-Step Sequential Method: Solvent–Morphology Relationship," *Materials* **16**, no. 3 (2023), https://doi.org/10.3390/ma16031049.

PubMed | Web of Science® | Google Scholar

42 F. Ma, J. Li, W. Li, N. Lin, L. Wang, and J. Qiao, "Stable *α*/*δ* Phase Junction of Formamidinium Lead Iodide Perovskites for Enhanced Near-Infrared Emission," *Chemical Science* **8**, no. 1 (2017): 800–805, https://doi.org/10.1039/c6sc03542f.

CAS | PubMed | Google Scholar

43 T. Zhu and X. Gong, *Low-Dimensional Perovskite Materials and Their Optoelectronics*. (InfoMat. Blackwell Publishing Ltd. October 1, 2021), 1039–1069, https://doi.org/10.1002/inf2.12211

Google Scholar

44 O. E. Solis, M. Mínguez-Avellán, P. F. Betancur, et al., "Adjusting the Crystallization of Tin Perovskites through Thiophene Additives for Improved Photovoltaic Stability," *Acs Energy Letters*.

Back

PubMed | Web of Science® | Google Scholar

45 J. Kim, A. J. Yun, B. Gil, Y. Lee, and B. Park, "Triamine-Based Aromatic Cation as a Novel Stabilizer for Efficient Perovskite Solar Cells," *Advanced Functional Materials* **29**, no. 44 (2019), https://doi.org/10.1002/adfm.201905190.

Web of Science® | Google Scholar

Download PDF

ABOUT WILEY ONLINE LIBRARY

Privacy Policy
Terms of Use
About Cookies
Manage Cookies
Accessibility
Wiley Research DE&I Statement and Publishing Policies

HELP & SUPPORT

Contact Us
Training and Support
DMCA & Reporting Piracy
Sitemap

OPPORTUNITIES

Subscription Agents
Advertisers & Corporate Partners

CONNECT WITH WILEY

The Wiley Network
Wiley Press Room

View PDF